CHAPTER IV
RESULTS AND DISCUSSION

4.1 Rheological Characterization

4.1.1 G' and G" versus Frequency

Figures 4.1-4.8 show the storage modulus, G', and the loss modulus, G", as a function of the frequency, ω. The liquid-like terminal zone was observed for all high density polyethylene (HDPE) melts but the entanglement plateau zone was not found on this frequency range due to the frequency limitation of the instrument (100 rad/s) and therefore G' and G" were presumably in the terminal zone. Lowering temperature led to higher G' and G" values obtained.

4.1.2 Master Curves

Master curves were obtained through measurements of G' and G" as a function of frequency at various temperatures. The storage modulus and loss modulus curves at different temperatures were shifted horizontally by using the time-temperature superposition and shifted vertically for density correcting as temperature was varied. Master curves were obtained at the reference temperatures of 160 ^{0}C, 180^{0}C and 200 ^{0}C for H5604F HDPE and H5840B HDPE as shown in Figures 4.9-4.11 and 4.13-4.15 respectively. For H5690S HDPE and H5818J HDPE, master curves were obtained only at the reference temperature of 180 ^{0}C as shown in Figures 4.12 and 4.16 respectively. The horizontal shift factor, a_T, and the vertical shift factor, b_T, are shown in Figures A15-22. However scattering of G' at low $a_T\omega$ of the master curve was possibly caused by the limitation of the transducer used on measuring the low values of torque as shown in Figures 4.13-4.16.

For H5604F HDPE and H5690S HDPE, we obtained the crossover moduli and the crossover frequencies directly when materials were in the molten state because their molecular weights are sufficiently high, $M_w \geq 2.4x10^5$ g/mol. But for H5840B HDPE and H5818J HDPE, we cannot see the crossover moduli and crossover frequencies directly above the melting temperature, T_m, because of the low molecular weight effect. Therefore data extrapolation was carried out to determine the extrapolated crossover modulus, $G_{c,ext}$ and the extrapolated crossover frequency, $\omega_{c,ext}$, as shown in Figures 4.17-4.20. The crossover modulus, the crossover frequency, the extrapolated crossover modulus and the extrapolated crossover frequency are tabulated in Table 4.1 and Table 4.2.

Table 4.1 The crossover modulus, G_c, and the crossover frequency, ω_c, at the different reference temperatures for H5604F HDPE and H5690S HDPE

Materials	T_{ref} (^{0}C)	G_c (dyn/cm^2)	ω_c (rad/s)
H5604F	160	$1.48x10^5$	0.14
	180	$1.34x10^5$	0.47
	200	$8.01x10^4$	0.51
H5690S	180	$3.22x10^5$	11.3

Table 4.2 The extrapolated crossover modulus, $G_{c,ext}$, and the extrapolated crossover frequency, $\omega_{c,ext}$ at different reference temperatures for H5840B HDPE and H5818J HDPE

Materials	T_{ref} (^{0}C)	$G_{c,ext}$ (dyn/cm^2)	$\omega_{c,ext}$ (rad/s)
H5840B	160	9.82×10^5	210
	180	9.17×10^5	236
	200	8.87×10^5	251
H5818J	180	1.09×10^6	613

Figures A9-A12 show the plots of G_c and ω_c as a function of molecular weight and polydispersity respectively at the reference temperature of 180 ^{0}C. G_c and ω_c steadily decrease as molecular weight and polydispersity increase.

But for the effect of temperature, G_c and ω_c approximately follow power laws as shown in Figures A13-A14. The scaling exponents on the temperature effect are tabulated in Table 4.3, where the scaling exponent x and y are defined as

$$G_c \alpha (\text{Temperature})^x, \quad (4.1)$$

and

$$\omega_c \alpha (\text{Temperature})^y. \quad (4.2)$$

I19358799

Table 4.3 The scaling exponent of the crossover modulus and the crossover frequency on the effect of temperature

Material	X value	Y value
H5604F HDPE	-2.71	5.88
H5840B HDPE	-0.46	0.80

Variation in the crossover modulus and the crossover frequency are often attributed to molecular weight distribution determination (Dealy and Wissbrun, 1990) but there is no report on the determination of the crossover modulus and the crossover frequency on molecular weight, polydispersity and temperature.

4.2 Slip Determination

4.2.1 Apparent Flow Curves

The apparent flow curve is the plot of the wall shear stress, τ_w, versus the apparent shear strain rate, γ_{app}, first obtained by the capillary rheometer without any corrections to the shear strain rate. The apparent flow curves were obtained from a capillary die number 1860, which has a length of 50.19 mm, a diameter of 1.25 mm and l_C/d_C is equal to 40.15.

a) Effect of Molecular Weight and Polydispersity

Figure 4.21 shows the apparent flow curves of four different grades of HDPE (H5640F, H5840B, H5818J and H5690S) melts at the temperature of 180 ^{0}C. The shear stress steadily increases as the shear strain rate increases. Each flow curve exhibits a bending of the flow curve at a high shear stress, the well-known shear thinning behavior (Tadmor and Gogos,

1979). Molecular weight dependence can be obviously observed in this figure; each flow curve simply shifts to a higher shear stress as the molecular weight increases. In addition, there is an interesting occurrence, an oscillating stress regime or a bifurcation pattern was found when the molecular weight was greater than $2.4x10^5$ g/mol. Both H5604F HDPE and H5690S HDPE flow curves exhibited distinct bendings and oscillating regimes although their molecular weights of these two grades were nearly identical. Difference in behavior could be attributed to the difference in polydispersity of the materials.

b) Effect of Temperature

Figures 4.22 and 4.23 show the temperature dependence of viscosity or shear stress of H5604F HDPE and H5840B HDPE respectively. The shifting of the apparent flow curve to slightly lower shear stress for the entire range of shear strain rate was typically found as temperature was increased. At a higher temperature, polymer chains were able to move and flow easily so it needed a lower force to push the material flow in the capillary die. For the H5604F HDPE, the oscillating stress regime was found at the temperatures of 160, 180 and 200 ^{0}C. But for H5840B HDPE, the oscillating stress regime was found only at the temperature of 160 ^{0}C. A threshold in shear stress was required for the oscillating regime of H5840B HDPE because at 160 ^{0}C, the values of shear stress were greater than the others.

4.2.2 Oscillating Stress Regime

The oscillating stress regime consists of upper and lower values of stresses that can be observed from fluctuations of the piston load as a function of time (in a periodic fashion) at a fixed apparent shear strain rate. It is known that the oscillation frequency is normally a function of shear strain rate, which

is close to the inverse of the longest molecular relaxation time of the bulk polymer, and the oscillating stress threshold is proportional to the plateau modulus of polymer melts (Mhetar and Archer, 1998). The upper load limit refers to the maximum load in the cycle. Similarly, the lower load limit refers to the minimum load in the cycle. The upper load limit corresponded to the end of the sharkskin/smooth segment, this regime still underwent the stick or entanglement state. At the lower load limit, an extrudate distortion manifested an end of the melt fracture section in which slip or plug-like profile was promoted (Leonov and Prokunin, 1994).

a) Hysteresis

Hysteresis or memory effect of the oscillating stress regime was investigated by comparing two modes of controlling plunger velocity: (I) Step up, the plunger velocity was varied from a low value to a high value; (II) Step down, opposite to the first type, the plunger velocity was varied from a high value to a low value as shown in Figure 4.24. The onset shear strain rate of the step up experiment was almost identical to the onset shear strain rate of the step down experiment. Moreover the terminal shear strain rate of the step up experiment was also close to the terminal shear strain rate of the step down experiment which confirms a lack of the memory effect for the oscillating stress regime for this HPDE (H5604F) melt studied. The shear strain rate at the onset and at the terminal point of the oscillating stress regime were obtained by performing at least 3 experiments as shown in Table 4.4.

Table 4.4 The onset and the terminal shear strain rates of the oscillating stress regime of H5604F HDPE at the temperature of 180 ^{0}C

Run type	Onset shear strain rate (s^{-1})	Std. (s^{-1})	Terminal shear strain rate (s^{-1})	Std. (s^{-1})
Step up	403.75	4.7	498.75	8.5
Step down	402.50	5.0	501.25	8.5

b) Effect of Molecular Weight and Polydispersity

The plot of wall shear stress versus apparent shear strain rate in the oscillating stress regime of two HDPE (H5604F and H5690S) melts at the temperature of 180 ^{0}C is shown in Figure 4.25. The weight average molecular weights (M_w) of H5604F HDPE and H5690S HDPE melts are nearly identical: $2.6x10^5$ and $2.4x10^5$ g/mol, respectively. However their polydispersities are quite different; 77.4 and 4.1 respectively. It can be seen that the magnitude of the oscillating stress regime of H5604F HDPE is typically $0.2x10^6$ dyn/cm^2 whereas the magnitude of the oscillating stress regime of the narrow polydispersity HDPE (H5690S) melt is typically $1.0x10^6$ dyn/cm^2.

c) Effect of Temperature

Figure 4.26 shows the oscillating stress regimes on the plot of wall shear stress versus apparent shear strain rate of the high molecular weight HDPE (H5604F) melt at the temperatures of 160, 180 and 200 ^{0}C. It can be seen clearly that the magnitude of the oscillating became smaller as the operating temperature was increased. In addition, the oscillating stress regime also shifted to higher wall shear stress and higher apparent shear strain rate as temperature was increased.

4.2.3 The Critical Shear Stress (τ^*)

a) Effect of Molecular Weight and Polydispersity

Slip velocity is a well known function of the wall shear stress. Figures 4.27a-d show plots of slip velocity versus shear stress for all HDPE melts at the temperature of 180 ^{0}C. Three different regimes were observed when the molecular weight was greater than $2.4x10^5$ g/mol (H5604F HDPE and H5690S HDPE). For the lower molecular weight HDPE (H5840B and H5818J) melts, only two regimes were found. Regime I can be identified with entangled slip regime. Regime II can be identified with marginal regime and regime III can be identified with rouse regime. These regimes were originally proposed by Brochard and de Gennes (1992).

Figures 4.28 and 4.29 show plots of slip velocity versus wall shear stress of four different molecular weight HDPE melts at the temperature of 180 ^{0}C. The critical shear stress, τ^*, or the shear stress at the onset of slip velocity was determined by the extrapolation of plotting the slip velocity versus shear stress in only entangled slip regime. The critical shear stresses for all HDPE melts at the temperature of 180 ^{0}C and the critical shear stresses of Kwaengsobha (1998) results are tabulated in Table 4.5.

Table 4.5 Comparison of the critical shear stresses obtained in our experiment: H5604F HDPE; H5840B HDPE; H5818J HDPE and H5690S HDPE at temperature of 180 ^{0}C in Kwaengsobha (1998) experiment: H5690S HDPE; H6205JU HDPE; L2009F LLDPE; L2020F LLDPE and M3204RU LLDPE at the temperature of 190 ^{0}C

Material	Temperature (^{0}C)	M_w (g/mol)	Polydispersity (M_w/M_n)	τ^* (dyn/cm^2)
H5604F HDPE	180	$2.66x10^5$	77	$1.09x10^6$
H5840B HDPE	180	$1.33x10^5$	20	$5.01x10^5$
H5818J HDPE	180	$6.39x10^4$	24	$4.13x10^5$
H5690S HDPE	180	$2.40x10^5$	4.1	$6.63x10^5$
H5690S HDPE (Kwaengsobha)	190	$2.40x10^5$	4.1	$1.19x10^6$
H6205JU HDPE (Kwaengsobha)	190	$9.80x10^4$	13	$8.80x10^5$
L2009F LLDPE (Kwaengsobha)	190	$8.90x10^4$	9.8	$1.08x10^6$
L2020F LLDPE (Kwaengsobha)	190	$5.50x10^4$	4.2	$1.03x10^6$
M3204RU LLDPE (Kwaengsobha)	190	$3.30x10^4$	8.3	$9.60x10^5$

The critical shear stress, τ^*, increases with molecular weight in all of the materials studied. This finding is consistent with the results of Kwaengsobha (1998) as shown in Figure 4.30. For HDPE and LLDPE of Kwaengsobha's experiments at the temperature of 190 ^{0}C, τ^* slightly increases as the molecular weight increases.

For the effect of polydispersity, using H5604F HDPE and H5690S HDPE, τ^* increases as the polydispersity increases as tabulated in Table 4.5.

b) Effect of Temperature

Figures 4.31a-c and 4.32a-c show plots of slip velocity versus wall shear stress of H5604F HDPE and H5840B HDPE at the temperatures of 160, 180 and 200 ^{0}C. Again, three distinct regimes were found which were identified previously. Both H5604F HDPE and H5840B HDPE melts show three and two regimes respectively as the temperature was varied.

The dependence on the temperature of the critical shear stress, τ^*, was determined for H5604F HDPE and H5840B HDPE melts at three different temperatures as shown in Figures 4.33 and 4.34. The τ^* data of H5604F HDPE and H5840B HDPE melts studied are tabulated in Table 4.6.

Table 4.6 The critical shear stress comparison between our experiment: H5604F HDPE and H5840B HDPE with Kwaengsobha (1998) experiment: L2020F LLDPE and H5690S HDPE at various temperatures

Material	M_w (g/mol)	Polydispersity (M_w/M_n)	Temperature (^0C)	τ^* (dyn/cm^2)
H5604F HDPE	$2.66x10^5$	77	160	$1.57x10^6$
			180	$1.09x10^6$
			200	$8.72x10^5$
H5840B HDPE	$1.33x10^5$	20	160	$9.02x10^5$
			180	$5.93x10^5$
			200	$4.56x10^5$
L2020F LLDPE (Kwaengsobha)	$5.5x10^4$	4.2	170	$1.14x10^6$
			190	$1.03x10^6$
			210	$0.99x10^6$
			230	$0.84x10^6$
H5690S HDPE (Kwaengsobha)	$2.40x10^5$	4.1	190	$1.19x10^6$
			210	$0.99x10^6$
			230	$0.98x10^6$

Data in Table 4.6 show that the critical shear stress, τ^*, steeply decreases as temperature increases for both H5604F HDPE and H5840B HDPE melts. The results are quite consistent with Kwaengsobha's data as shown in Figure 4.35.

4.2.4 Extrapolation Length

The extrapolation length (b) was calculated by using Equation 3.7 as shown below

$$b \equiv \frac{V_s}{\gamma_{app,s}}. \tag{3.7}$$

The b value plays an importance role for the surface defects in the polymer processing when compared with the diameter size of the adsorbed polymer chains at the interface (Mhetar and Archer, 1998; Leonov and Prokunin, 1994).

a) Effect of Molecular Weight and Polydispersity

Figures 4.36 and 4.37 illustrate the extrapolation length as a function of slip velocity of four different molecular weight HDPE melts at the temperature of 180 ^{0}C. Again, three different slip regimes were observed as qualitatively identified by Brochard and de Gennes (1992):

(I) Entangled Slip Regime

The extrapolation length is independent of the slip velocity. Figure 4.38 shows a plot between b_0 versus the weight average molecular weight, M_w. Figure 4.38 shows that the b_0 value decreases as the molecular weight increases with a negative scaling exponent of -0.36. This scaling exponent is not different from the scaling exponent value predicted by de Gennes as shown in Equation 1.3:

$$b_0 \cong \frac{1}{\upsilon R_0} = \frac{1}{\upsilon a\sqrt{N}} \tag{1.3}$$

and
$$N = M_w/M_0 \tag{4.3}$$

where M_0 is the monomer weight,

so
$$b_0 \alpha \frac{1}{M_w^{1/2}}. \tag{4.4}$$

Experimental results in Figure 4.38 are definitely in contrast to Archer's results (PBD), $b_0 \alpha M^{1.94}$, as shown in Table 4.7. The material structure, instrument and velocity profile were possibly the causes. Massey's experimental data (PDMS), however, proposed the role of attached

polymer molecules in wall slip that appear to be consistent with de Gennes and Kwaengsobha experiments.

For the effect of polydispersity, the value of b_0 increases as the polydispersity increases as tabulated in Table 4.8. The broader polydispersity polymer has more short chains (smaller M_w) in the system when compared with the narrow one; this smaller M_w amount possibly a rise to a higher value of b_0 according to the Equation 4.4.

Table 4.7 Comparison slip data of b_0 in the entangled slip regime of five experiments: HDPE, 180 ^{0}C; PBD, room temperature (Archer); PDMS, 23 ^{0}C (Massey); LLDPE, 190 ^{0}C (Kwaengsobha) and HDPE, 190 ^{0}C (Kwaengsobha) experiments

Experiment/instrument	M_w (g/mol)	Polydispersity (M_w/M_n)	b_0 (μm)
Experiment (2000) HDPE/capillary rheometer (180 ^{0}C)	$6.39x10^4$	25	25.8
	$1.33x10^5$	19	23.2
	$2.68x10^5$	77	13.5
Mhetar and Archer (1998) Polybutadiene/plane couette shear flow (Room temperature)	$6.99x10^4$	1.04	2.4
	$8.99x10^4$	1.04	3.5
	$1.33x10^5$	1.03	7.7
	$1.82x10^5$	1.03	12.5
	$2.15x10^5$	1.04	16.3
	$2.96x10^5$	1.04	39.2
	$5.41x10^5$	1.05	122.6
Massey *et al.* (1997) PDMS/plane couette shear flow (23 ^{0}C)	$6.08x10^5$	1.2	0.81
Kwaengsobha (1998) LLDPE/capillary rheometer (190 ^{0}C)	$3.30x10^4$	8.3	58.9
	$6.07x10^4$	4.2	71.4
	$8.70x10^4$	9.8	63.5
Kwaengsobha (1998) HDPE/capillary rheometer (190 ^{0}C)	$9.80x10^4$	13	87.1
	$2.40x10^5$	4.1	59.3

Table 4.8 b_0 of two HDPE (H5604F and H5690S) melts of different polydispersity at the temperature of 180 ^{0}C

Materials	M_w (g/mol)	Polydispersity (M_w/M_n)	b_0 (μm)
H5690S HDPE	$2.40x10^5$	4.1	8.3
H5604F HDPE	$2.68x10^5$	77	13.5

(II) Marginal Regime

For the three different molecular weight HDPE melts, the extrapolation length in this regime is a power law function of slip velocity as shown in Figure 4.36. As slip velocity and temperature were fixed, the high molecular weight HDPE (H5604F) melt had a high value of the extrapolation length because of its viscosity, according to Equation 4.5 (combination of Equation 1.4 and Equation 1.5) as shown below

$$b(V_s) = \frac{\eta V_s a N_e^{1/2}}{\upsilon kT}. \qquad (4.5)$$

The scaling exponent of these three molecular weights are in the range of 0.42-0.68 which deviate from the disentanglement model as shown in Equation 4.5 ($b \alpha V_s^1$). Massey *et al.* (1997) suggested an argument that the exponent of the power law dependence of b versus V_s in the intermediate nonlinear friction regime is smaller than one, and the departure from unity will increase with the molecular weight of the polymer melt. The polydispersity effect on the marginal regime is shown in Figure 4.37. It is independent of polydispersity because the exponents of power law for these two HDPE (H5604F and H5690S) melts are nearly identical to each other at 0.42.

(III) Rouse Regime

The extrapolation length in this regime is again independent on the slip velocity and remains at b_∞. For high molecular weight HDPE (H5604F and H5690S) melts, b_∞ was found to exist as shown in Figures 4.36 and 4.37. The value of b_∞ seems to increase as molecular weight increases in the millimeter order magnitude as shown in Figure 4.39. Equation 1.6 can be used to clearly explain the molecular weight dependence in this regime as shown below

$$b_\infty = a\left[\frac{\eta}{\eta_l}\right]. \qquad (1.6)$$

where η_l is the viscosity of the monomer liquid and η is the bulk viscosity of the polymer fluid. High molecular weight material normally leads to high bulk viscosity therefore we can see the increasing value of b_∞ as the molecular weight increases. For the effect of polydispersity, b_∞ value increases as the polydispersity increases as tabulated in Table 4.9. This is because a higher bulk viscosity can be obtained from the broader polydispersity as compared to the narrow one.

Table 4.9 b_∞ of two HDPE (H5604F and H5690S) melts of different polydispersity at the temperature of 180 ^{0}C

Materials	M_w (g/mol)	Polydispersity (M_w/M_n)	b_∞ (μm)
H5690S HDPE	$2.40x10^5$	4.1	20.7
H5604F HDPE	$2.68x10^5$	77	61.2

b) Effect of Temperature

Figure 4.40 illustrates three different regimes of the plot between the extrapolation length and the slip velocity of H5604F HDPE at the temperatures of 160, 180 and 200 ^{0}C. For H5840B HDPE, only two regimes were observed as shown in Figure 4.41. These regimes are qualitatively consistent with Brochard and de Gennes' disentanglement model:

(I) Entangled Slip Regime

The extrapolation length is independent of the slip velocity and remained at a typical value of extrapolation length (b_0). Temperature seems to have no effect on this regime for both H5604F HDPE and H5840B HDPE melts. The extrapolation length in this regime shows a single value of the extrapolation length (b_0) around 13.5 μm for H5604F HDPE and 23.2 μm for H5840B HDPE as shown in Figure 4.42. Even though temperature was varied, slip phenomena still existed in the same manner in this temperature range, between 160 ^{0}C to 200 ^{0}C, in agreement with Equation. 1.3:

$$b_0 \cong \frac{1}{\upsilon R_0} = \frac{1}{\upsilon a\sqrt{N}}. \qquad (1.3)$$

It can be seen that b_0 was predicted to be independent of the temperature. For Kwaengsobha's result (1998), she found that b_0 slightly dropped as the temperature increased for both HDPE and LLDPE melts as shown in Figure 4.42.

(II) Marginal Regime

Brochard and de Gennes' theory (1992) suggested that the extrapolation length is a linear function of slip velocity. The extrapolation length in marginal regime should be dependent of temperature as followed:
From Arrhenius equation,

$$\eta_0(T) = A_0 e^{\frac{Ea}{RT}} \qquad (4.6)$$

$$b(V_s) = \frac{A_0 e^{\frac{Ea}{RT}} V_s a N_e^{1/2}}{\upsilon kT}. \quad (4.7)$$

If V_s is fixed

$$b \cong \text{const} \times \frac{e^{\frac{Ea}{RT}}}{T}, \quad (4.8)$$

therefore

$$\log b \, \alpha \, \frac{1}{T} - \log T. \quad (4.9)$$

Our data suggested that b in marginal regime is nearly independent of temperature for H5604F HDPE and H5840B HDPE. This finding may be due to the grafting density parameter (υ) of Equation 4.7 in which it did not remain constant; possibly it varied with temperature. This grafting density, however, may have decreased linearly as temperature was increased which finally led to the temperature independence. The scaling exponents between b and V_s from the experiment are 0.42 and 0.46 for H5604F HDPE and H5840B HDPE, respectively whereas the disentanglement model's scaling exponent is equal to 1.

(III) Rouse Regime

The extrapolation length in this regime is again independent on the slip velocity and remains at b_∞ for all temperatures studied as shown in Figure 4.40. Scaling exponent of the disentanglement model can be expressed by combining Equations 1.6 and 4.6 as:

$$b_\infty \cong a\left[\frac{A_{0,\text{polymer}}}{A_{0,\text{monomer}}} \times \frac{e^{(E_{a,\text{polymer}} - E_{a,\text{monomer}})}}{RT}\right], \quad (4.10)$$

then

$$b_\infty \cong \frac{\text{constant}}{RT} \quad (4.11)$$

so finally

$$b_\infty \alpha T^{-1}, \quad (4.12)$$

Figure 4.43 shows b_∞ as a function of temperature of H5604F HDPE for the temperatures of 160, 180 and 200 ^{0}C. The scaling exponent of the correlation between b_∞ and temperature from experiment is about -1.21 which is in an approximate agreement with the disentanglement model (exponent of -1).

4.3 Normalization of Flow Curve

4.3.1 True Flow Curve

The apparent flow curve without slip was eventually obtained after the apparent flow curve was corrected by the Mooney analysis for the slip as shown in Figures A1-A8. These apparent flow curves without slip still need non-Newtonian correction; it is not the actual flow curve. The power law correction was used for this correction. Subsequently the true flow curve was obtained (Dealy and Wissbrun, 1990).

a) Effect of Molecular Weight and Polydispersity

Figures 4.44-4.47 show the true flow curves of four different HDPE (H5604F, H5840B, H5818J and H5690S) melts at temperature of 180 ^{0}C. For these true flow curves, shear stress steadily increases and shows a bending in the flow curve indicating the shear thinning behavior as apparent shear strain rate without slip increases. Three different power law indices were found, when the molecular weight was greater than 2.4×10^5 g/mol, for the H5604 HDPE and H5690S HDPE melts. Only two different power law regimes were observed for the low molecular weight HDPE (H5840B and H5818J) melts. The power law index and the power law correction for each regime, as shown in Figures 4.44-4.47, are tabulated in Table 4.10.

Table 4.10 Power law index and power law correction of four different HDPE (H5604F, H5840B, H5818J and H5690S) melts at temperature of 180 ^{0}C

Materials	Regime	Power Law Index (n)	Power Law Correction
H5604F HDPE	I	0.41	1.36
	II	0.18	2.14
	III	0.22	1.89
H5690S HDPE	I	1.02	0.99
	II	0.52	1.23
	III	0.32	1.53
H5840B HDPE	I	0.51	1.24
	II	0.25	1.75
H5818J HDPE	I	0.56	1.20
	II	0.41	1.36

b) Effect of Temperature

Figures 4.48-4.53 show the true flow curves of H5604F HDPE and H5840B HDPE at three different temperatures of 160, 180 and 200 ^{0}C. Three distinctive power law indices were obtained for the high molecular weight HDPE (H5604F) melt as the operating temperature was varied. For the low molecular weight HDPE (H5840B) melt, two distinctive power law regimes were found although the temperature was varied. The power law index and the power correction for each regime, as shown in Figures 4.48-4.53, are tabulated in Table 4.11.

Table 4.11 Power law index and power law correction for each regime of H5604F HDPE and H5840B HDPE at the temperatures of 160, 180 and 200 ^{0}C

Materials	Temperature (^{0}C)	Regime	Power Law Index (n)	Power Law Correction
H5604F HDPE	160	I	0.51	1.24
		II	0.23	1.83
		III	0.17	2.22
	180	I	0.41	1.36
		II	0.18	2.14
		III	0.22	1.69
	200	I	0.52	1.23
		II	0.24	1.79
		III	0.15	2.42
H5840B HDPE	160	I	0.84	1.04
		II	0.48	1.27
	180	I	0.51	1.24
		II	0.25	1.75
	200	I	0.76	1.07
		II	0.52	1.23

4.3.2 Normalized Flow Curve

After we normalized the shear stress, τ_w, by the crossover modulus, G_c, and converted the true shear strain rate to Weissenberg number, Wi, a dimensionless flow curve was eventually obtained (the values of G_c and ω_c are already tabulated in Tables 4.1 and 4.2).

a) Effect of Molecular Weight and Polydispersity

Figure 4.54 shows the normalized flow curve of three different molecular weight HDPE (H5604F, H5840B and H5818J) melts at the temperature of 180 ^{0}C. These normalized flow curves do not collapse well as we varied molecular weight. A bending is observed when the elasticity is predominant (Wi > 1). For the viscous zone, Wi < 1, a power law correlation between the normalized shear stress (τ_w/G_c) and Wi can be seen.

Figure 4.55 shows the normalized flow curve of two different polydispersity HDPE (H5604F and H5690S) melts at the temperature of 180 ^{0}C. The normalized flow curve shows that the narrower polydispersity melt is less elastic than the broad polydispersity melt. The deviations of these two curves appear when Wi is greater than 1 and again bending of curve originates at this point.

b) Effect of Temperature

Figures 4.56 and 4.57 show the normalized flow curves of H5604F HDPE and H5840B HDPE at three temperatures of 160,180 and 200 ^{0}C. It can be seen that the normalized flow curves approximately collapse at low Wi. When the Weissenberg number is greater than 1 (the elastic predominates), these normalized flow curves do not collapse as can be seen in case of the high molecular weight HDPE (H5604F) melt as temperature was varied

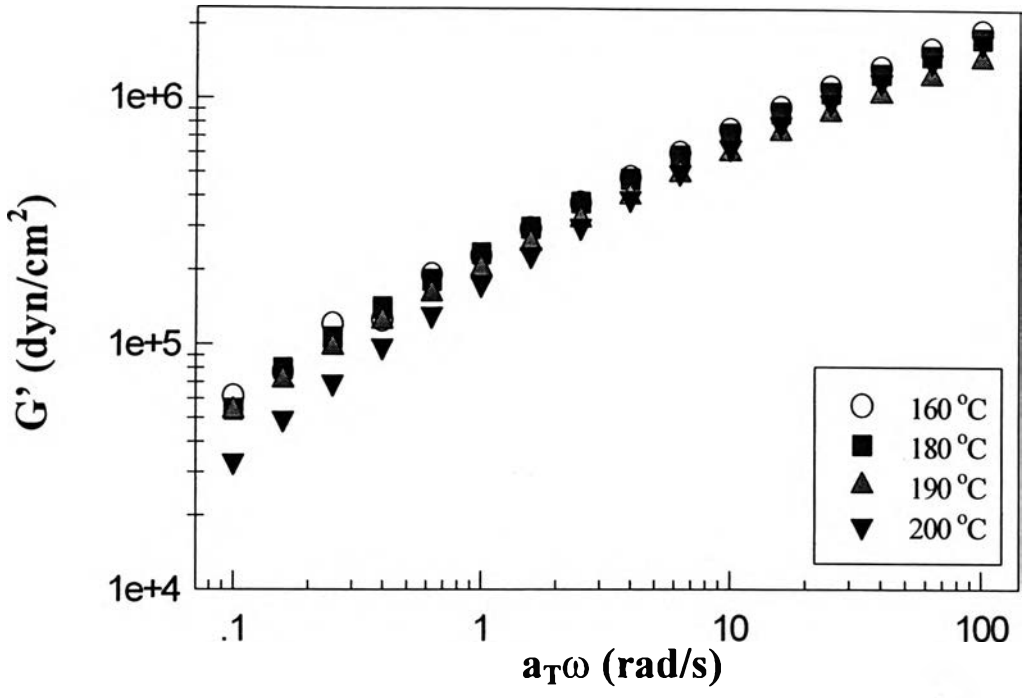

Figure 4.1 The storage modulus of H5604F HDPE melt as a function of frequency at strain amplitude equal to 10 and at different temperatures.

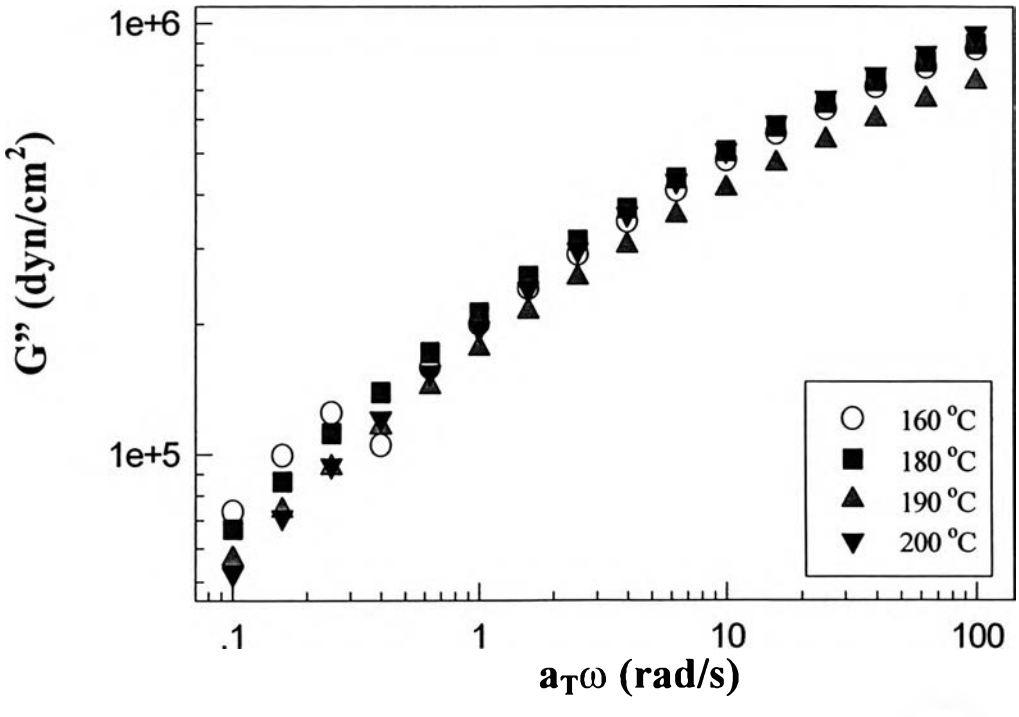

Figure 4.2 The loss modulus of H5604F HDPE melt as a function of frequency at strain amplitude equal to 10 and at different temperatures.

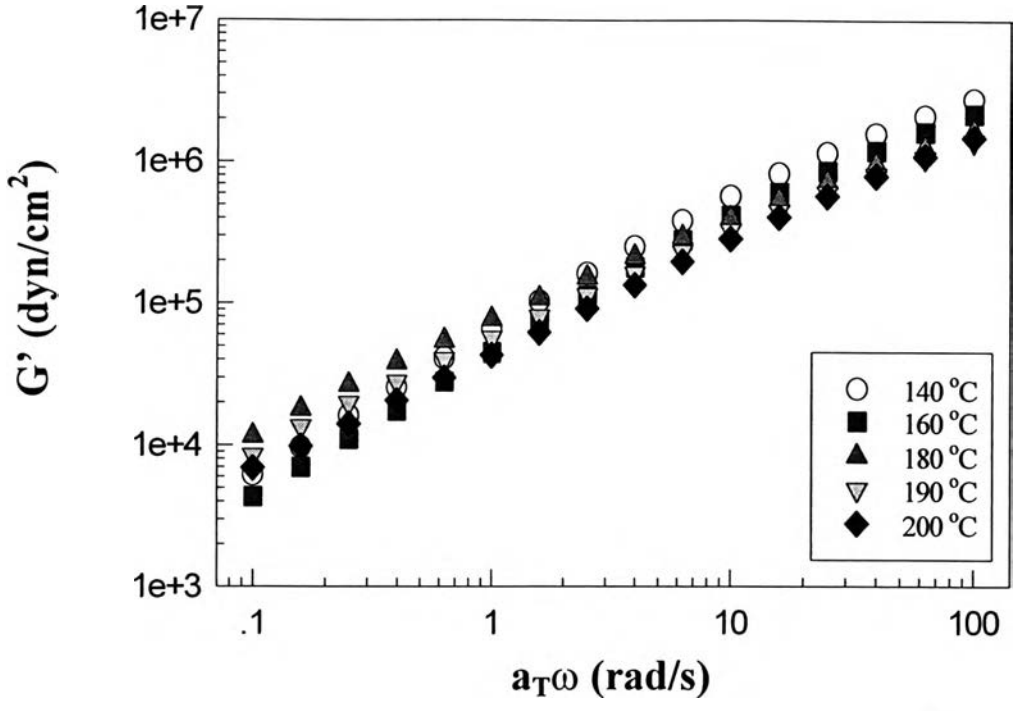

Figure 4.3 The storage modulus of H5690S HDPE melt as a function of frequency at strain amplitude equal to 10 and at different temperatures.

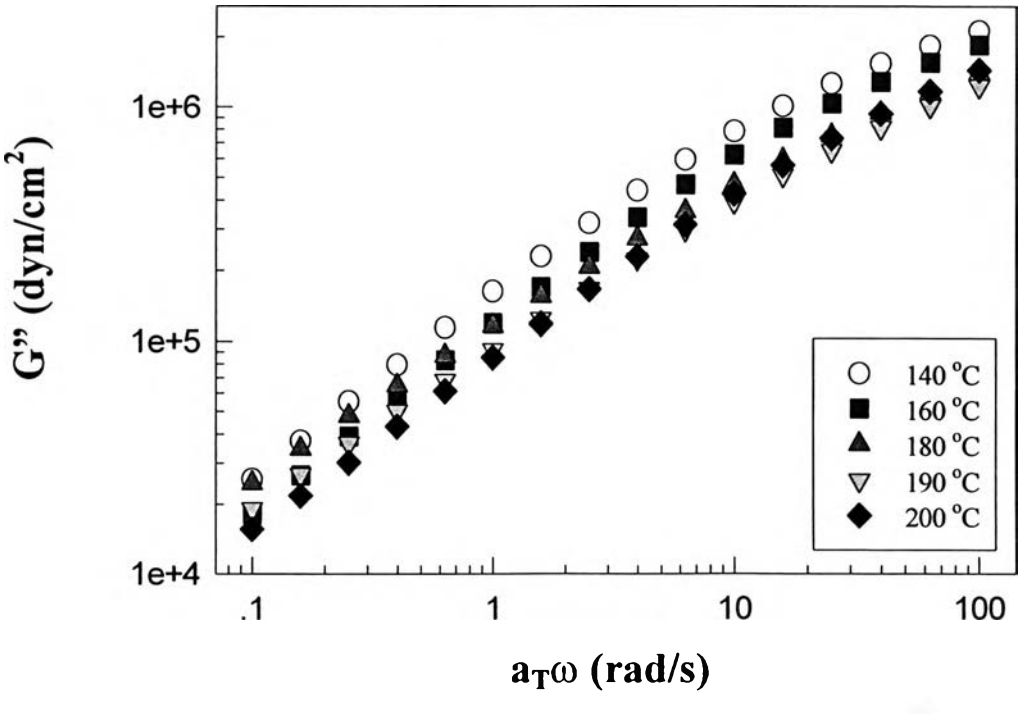

Figure 4.4 The loss modulus of H5690S HDPE melt as a function of frequency at strain amplitude equal to 10 and at different temperatures.

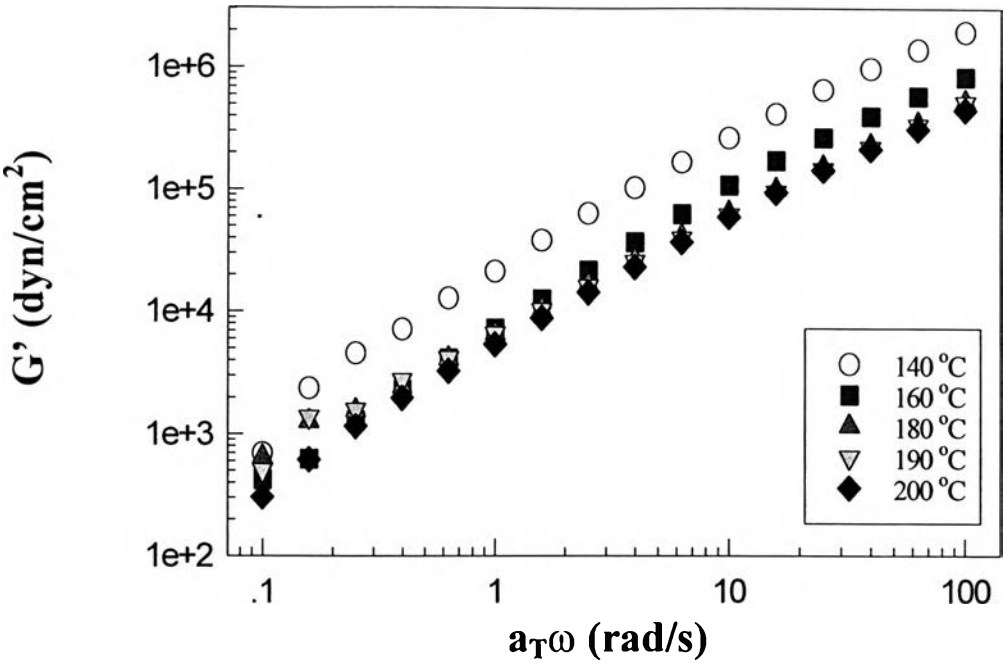

Figure 4.5 The storage modulus of H5840B HDPE melt as a function of frequency at strain amplitude equal to 10 and at different temperatures.

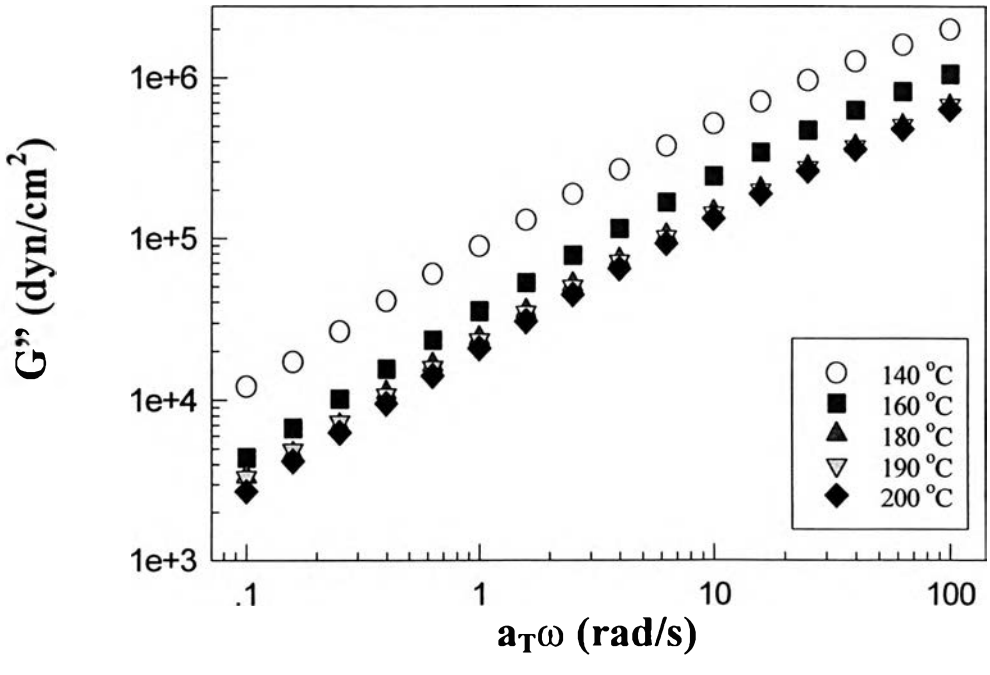

Figure 4.6 The loss modulus of H5840B HDPE melt as a function of frequency at strain amplitude equal to 10 and at different temperatures.

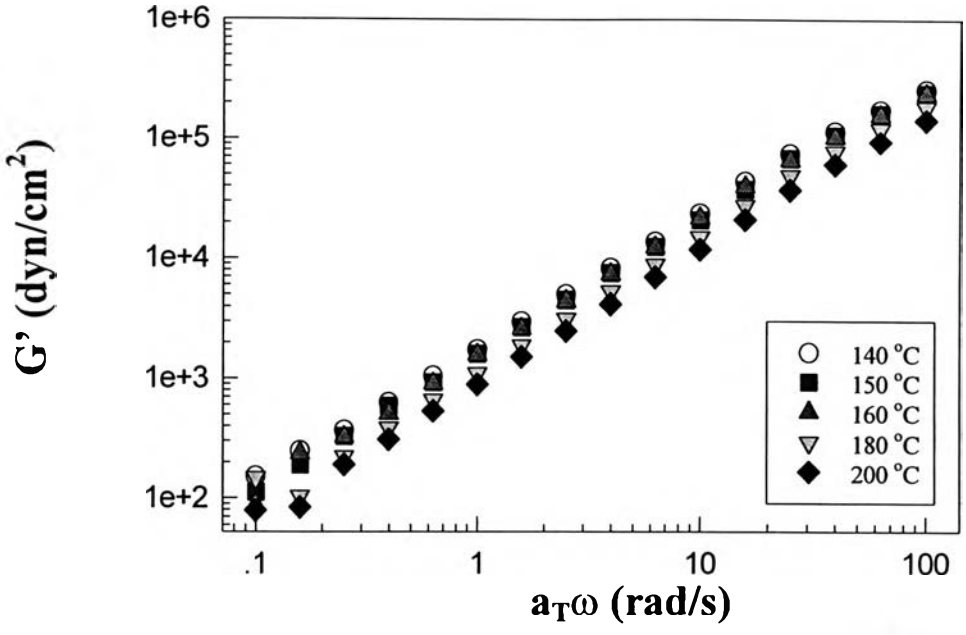

Figure 4.7 The storage modulus of H5818J HDPE melt as a function of frequency at strain amplitude equal to 10 and at different temperatures.

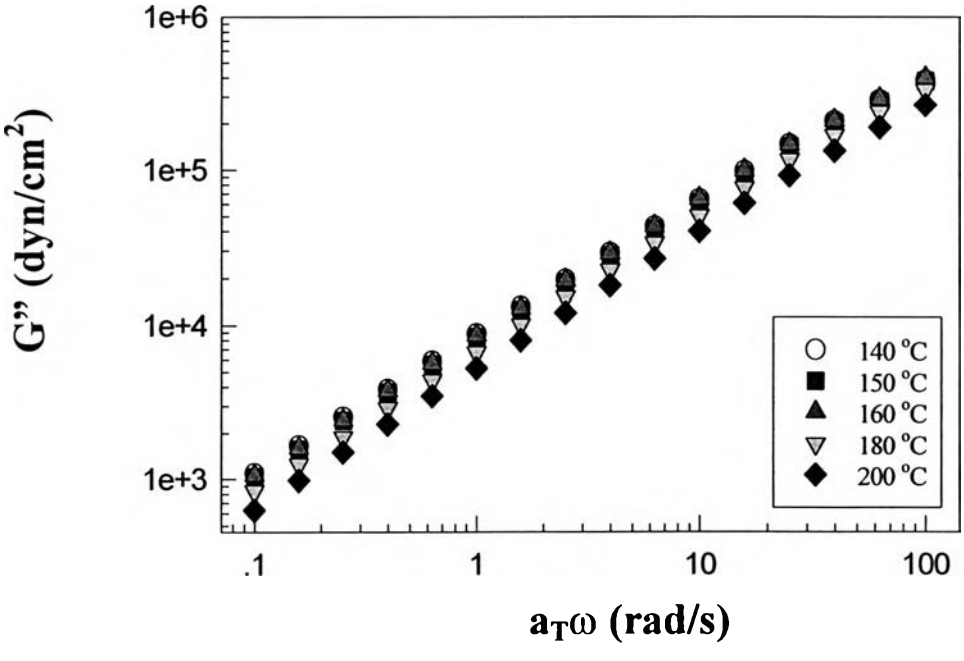

Figure 4.8 The loss modulus of H5818J HDPE melt as a function of frequency at strain amplitude equal to 10 and at different temperatures.

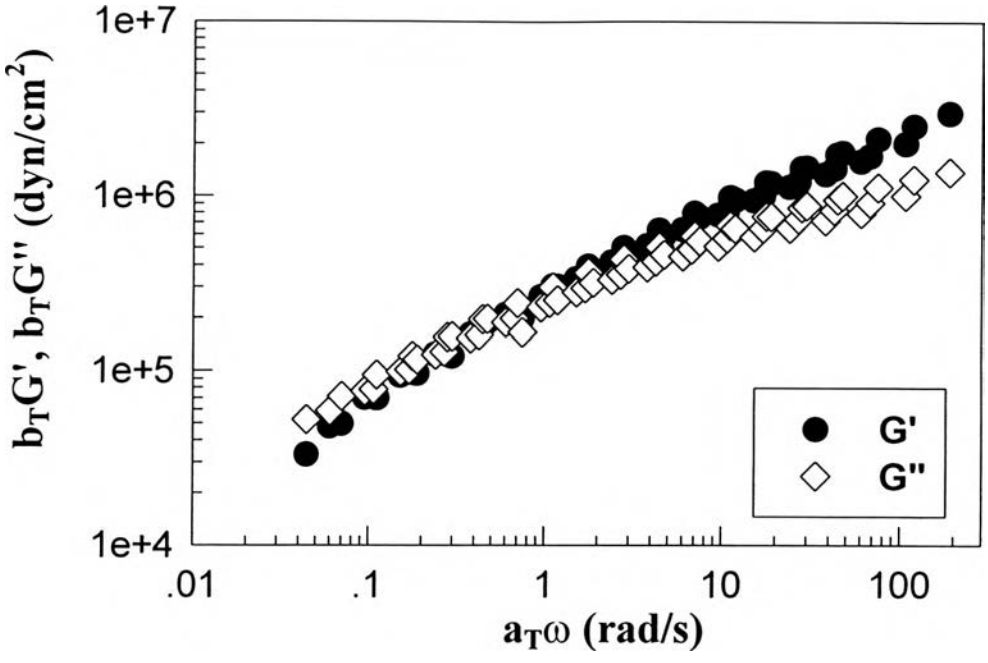

Figure 4.9 Master curve of H5604F HDPE melt at the reference temperature of 160 ^{0}C.

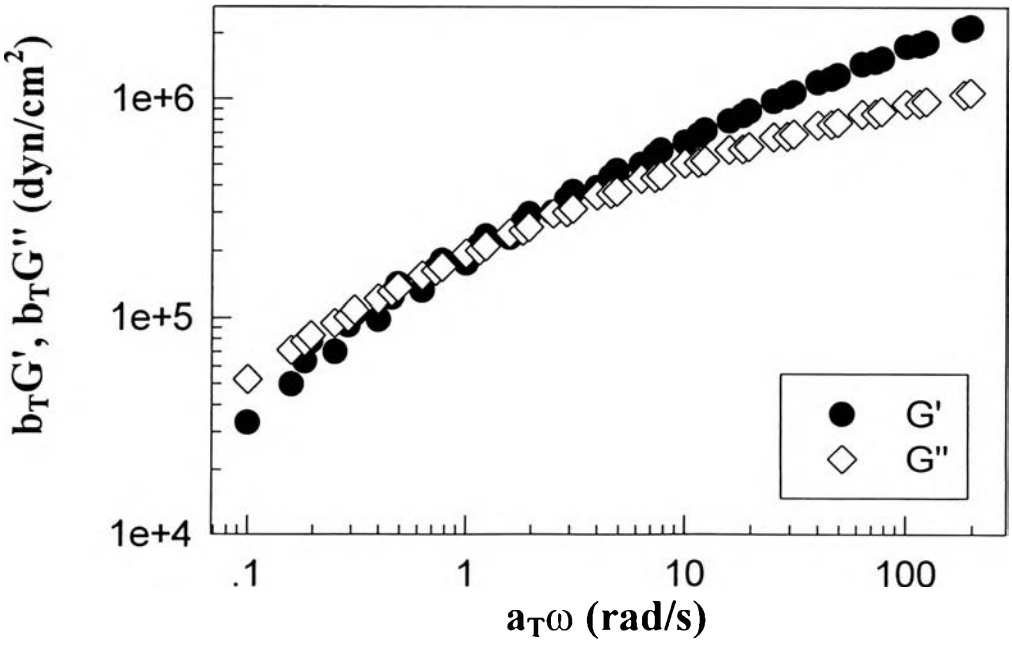

Figure 4.10 Master curve of H5604F HDPE melt at the reference temperature of 160 ^{0}C.

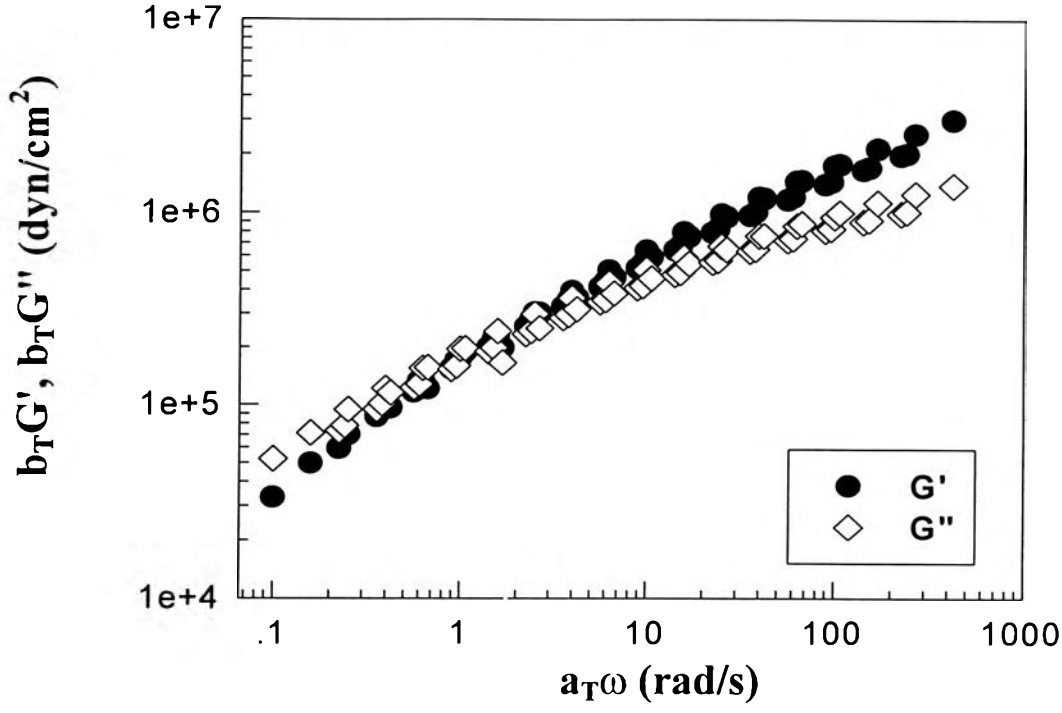

Figure 4.11 Master curve of H5604F HDPE melt at the reference temperature of 200 ^{0}C.

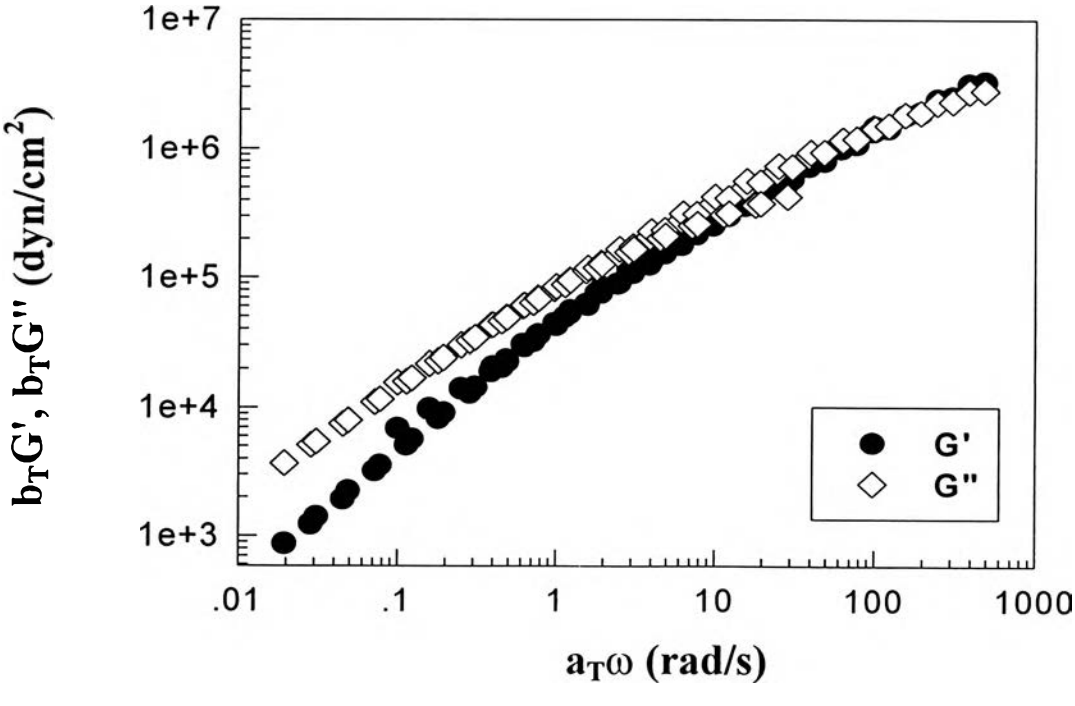

Figure 4.12 Master curve of H5690S HDPE melt at the reference temperature of 180 ^{0}C.

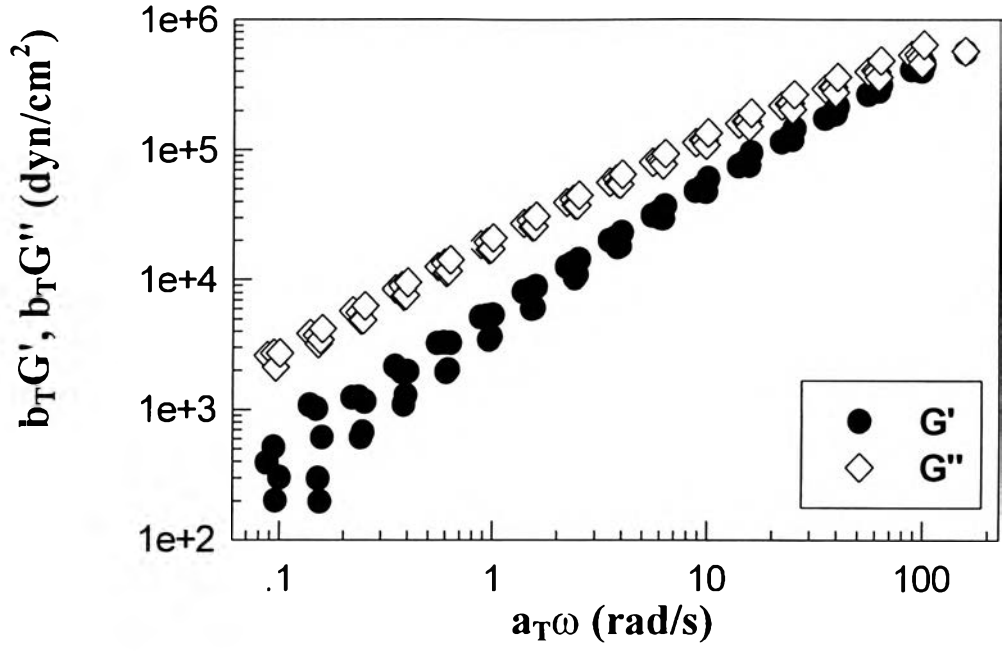

Figure 4.13 Master curve of H5840B HDPE melt at the reference temperature of 160 ^{0}C.

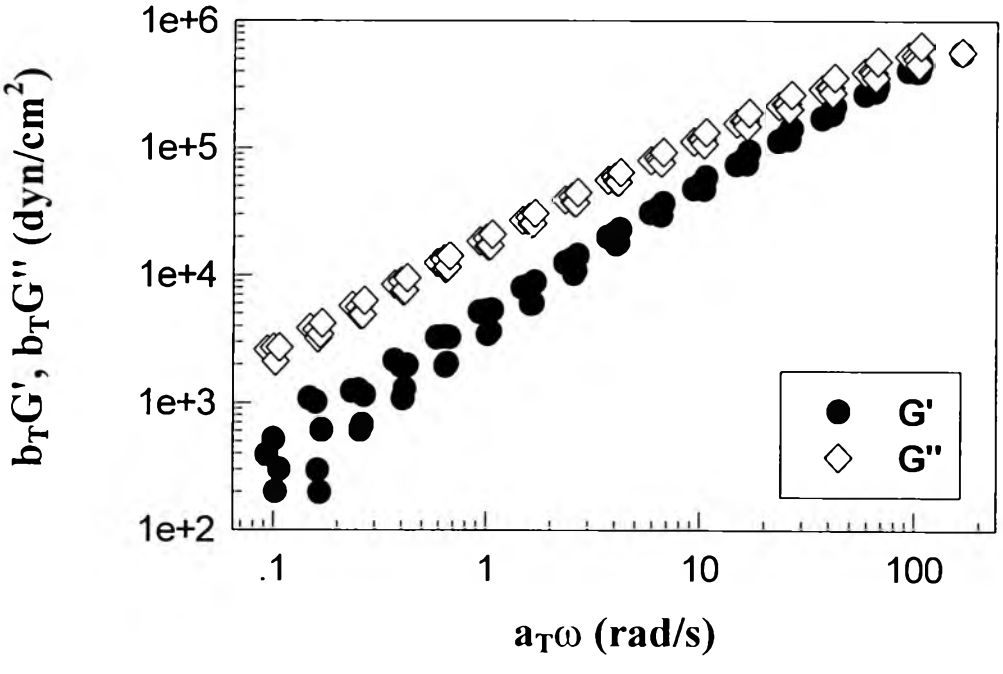

Figure 4.14 Master curve of H5840B HDPE melt at the reference temperature of 180 ^{0}C.

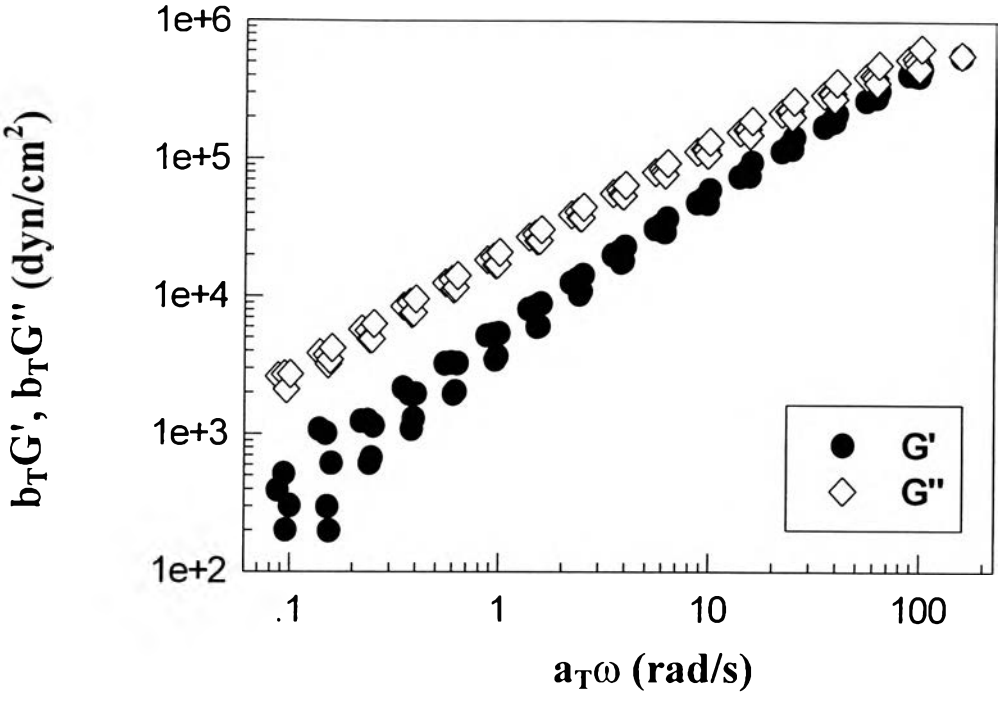

Figure 4.15 Master curve of H5840B HDPE melt at the reference temperature of 200 ^{0}C.

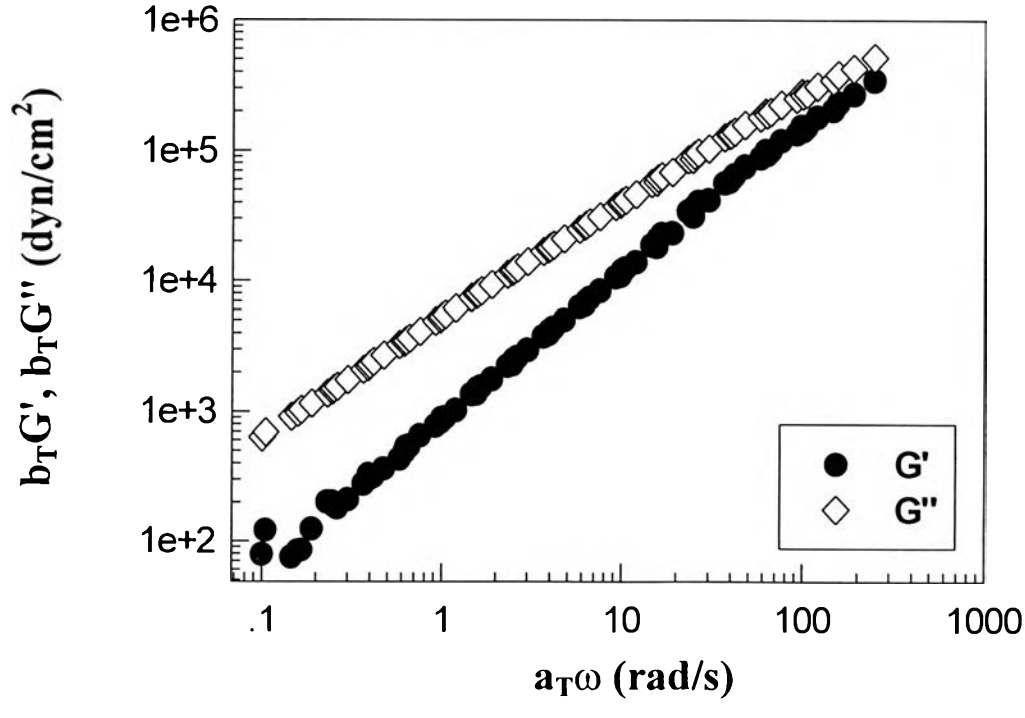

Figure 4.16 Master curve of H5818J HDPE melt at the reference temperature of 180 ^{0}C.

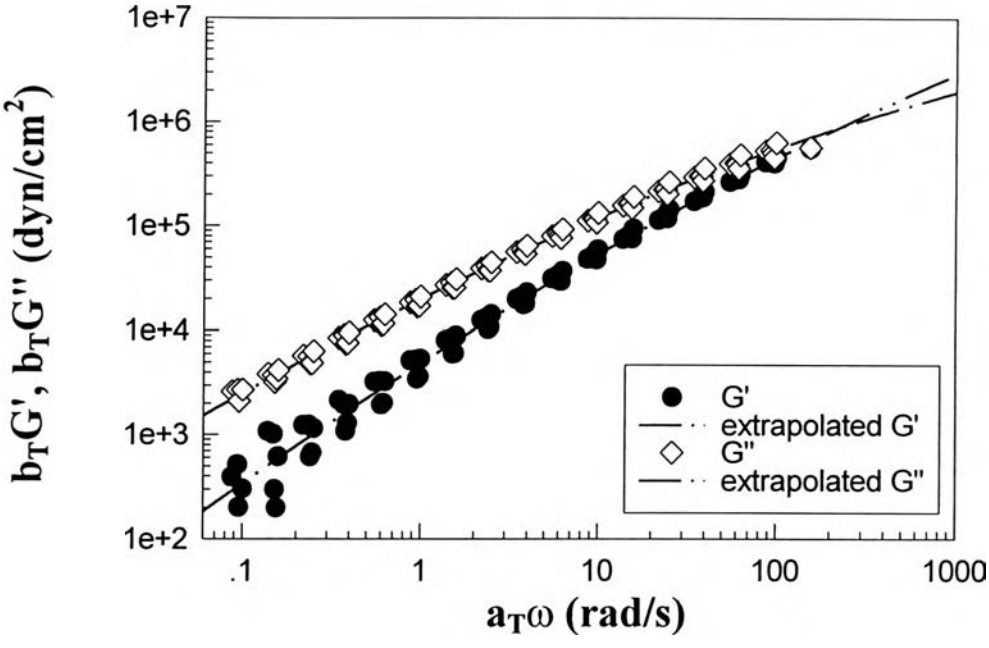

Figure 4.17 Master curve of H5840B HDPE melt and the extrapolated crossover modulus and the extrapolated crossover frequency at the reference temperature of 160 ^{0}C.

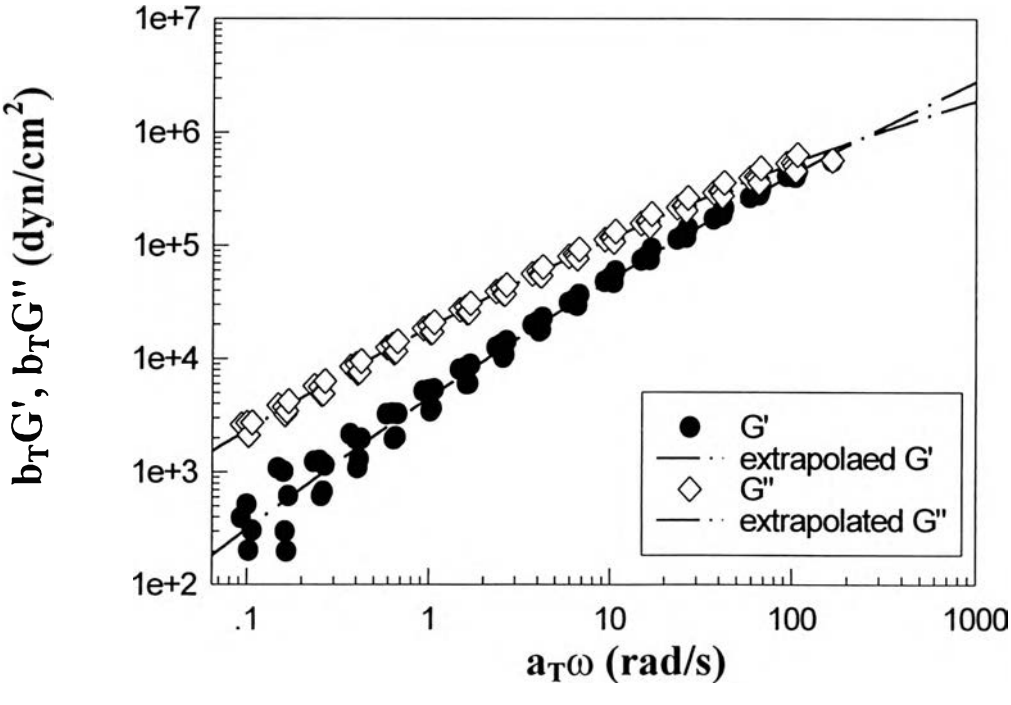

Figure 4.18 Master curve of H5840B HDPE melt and the extrapolated crossover modulus and the extrapolated crossover frequency at the reference temperature of 180 ^{0}C.

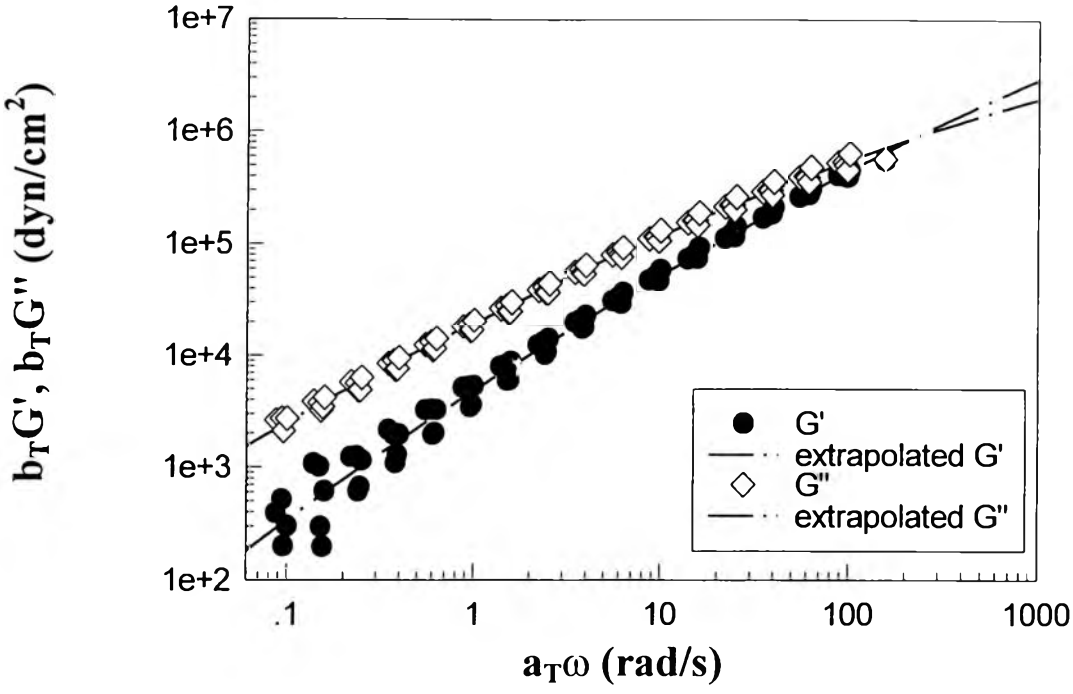

Figure 4.19 Master curve of H5840B HDPE melt and the extrapolated crossover modulus and the extrapolated crossover frequency at the reference temperature of 200 ^{0}C.

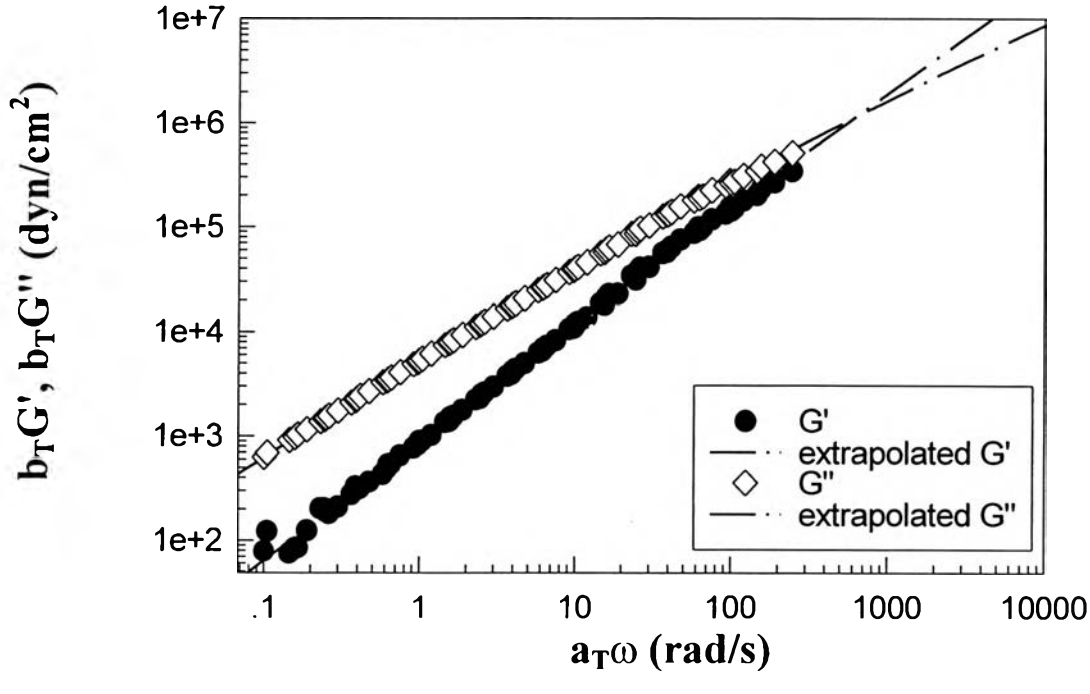

Figure 4.20 Master curve of H5818J HDPE melt and the extrapolated crossover modulus and the extrapolated crossover frequency at the reference temperature of 180 ^{0}C.

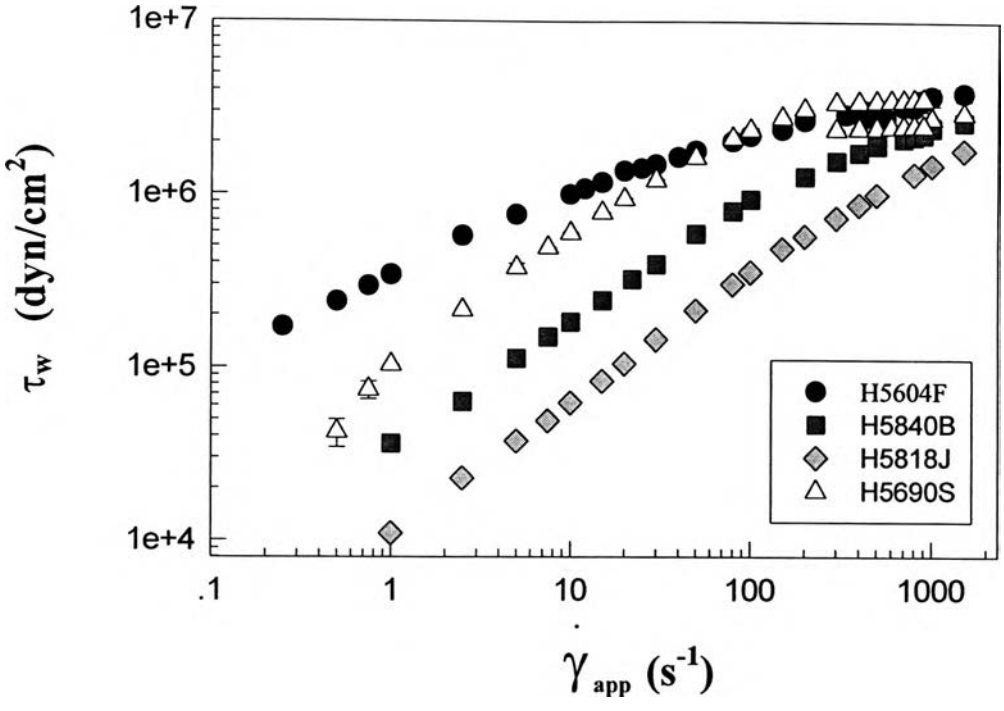

Figure 4.21 The apparent flow curve of four different HPDE (H5604F, H5840B, H5818J and H5690S) melts at the temperature of 180 ^{0}C.

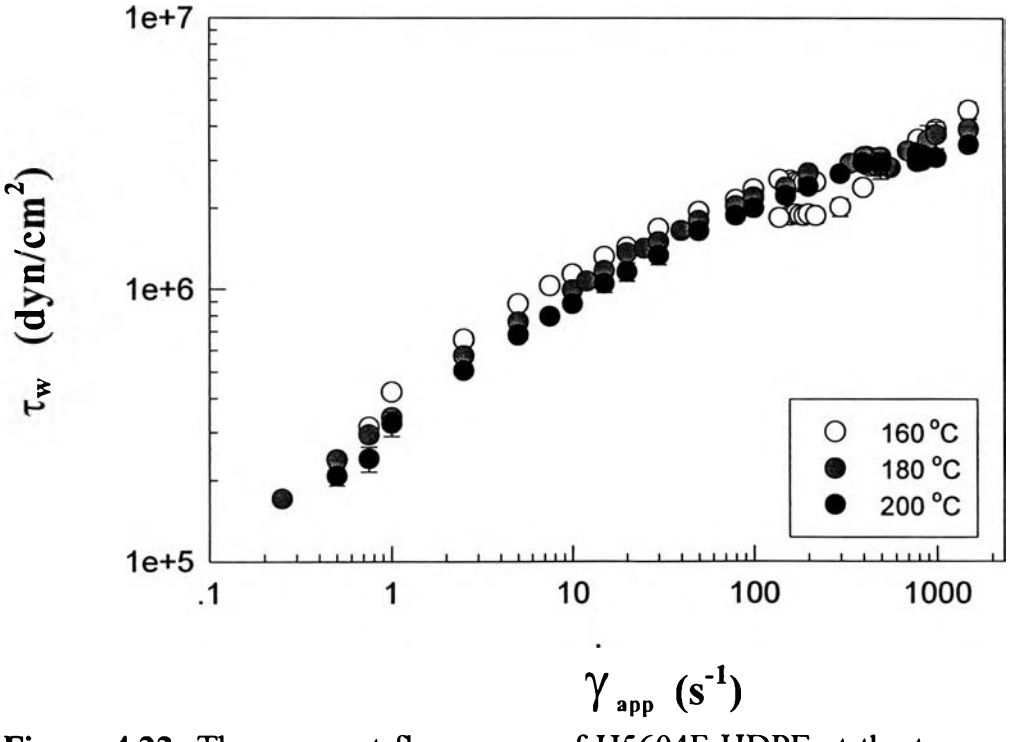

Figure 4.22 The apparent flow curve of H5604F HDPE at the temperatures of 160, 180 and 200 ^{0}C.

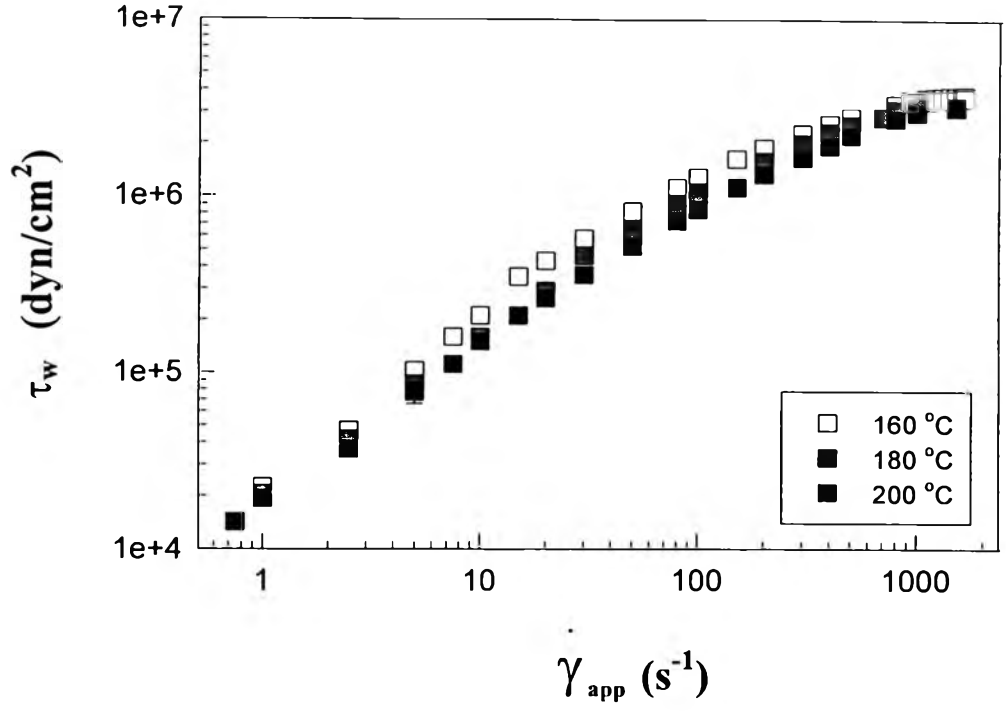

Figure 4.23 The apparent flow curve of H5840B HDPE at the temperatures of 160, 180 and 200 ^{0}C.

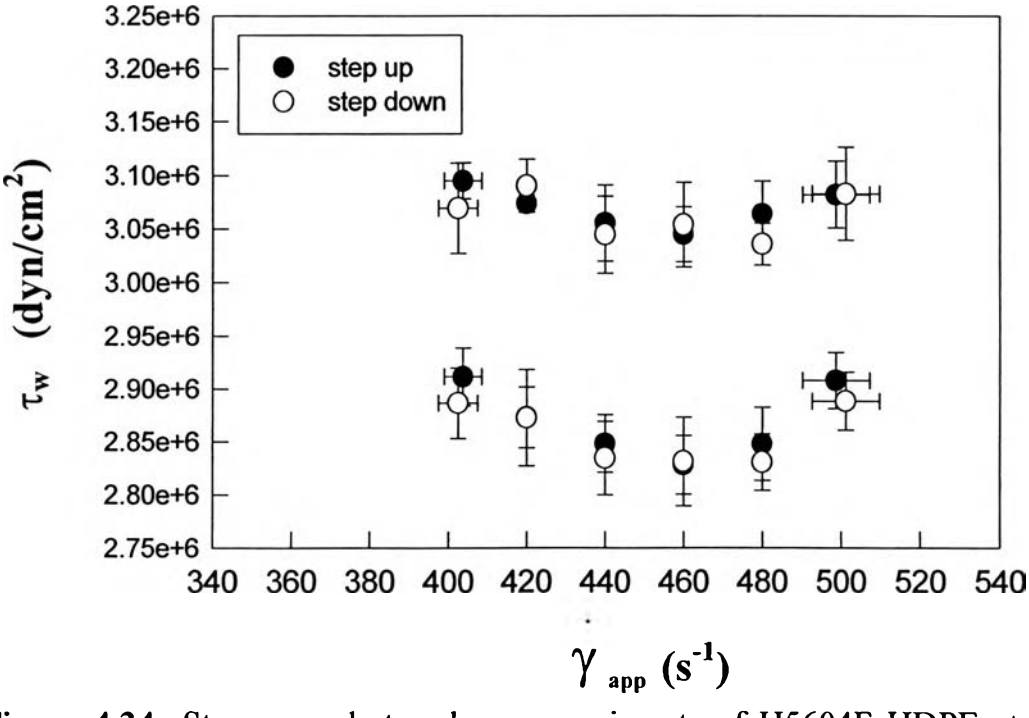

Figure 4.24 Step up and step down experiments of H5604F HDPE at the temperature of 180 ^{0}C.

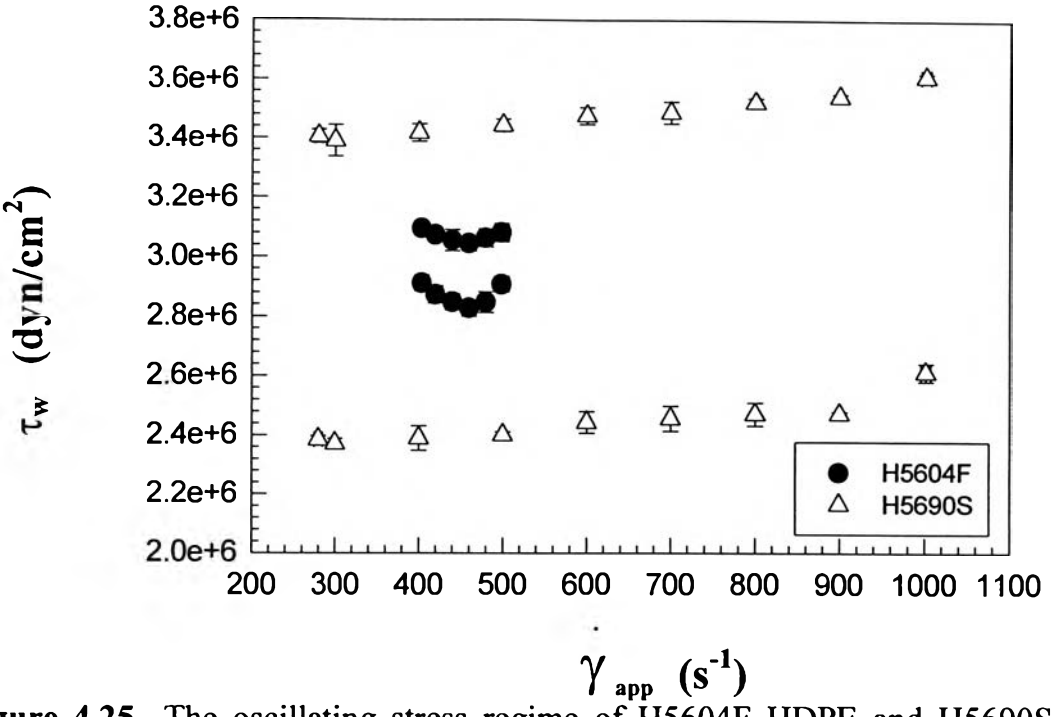

Figure 4.25 The oscillating stress regime of H5604F HDPE and H5690S HDPE at the temperature of 180 ^{0}C.

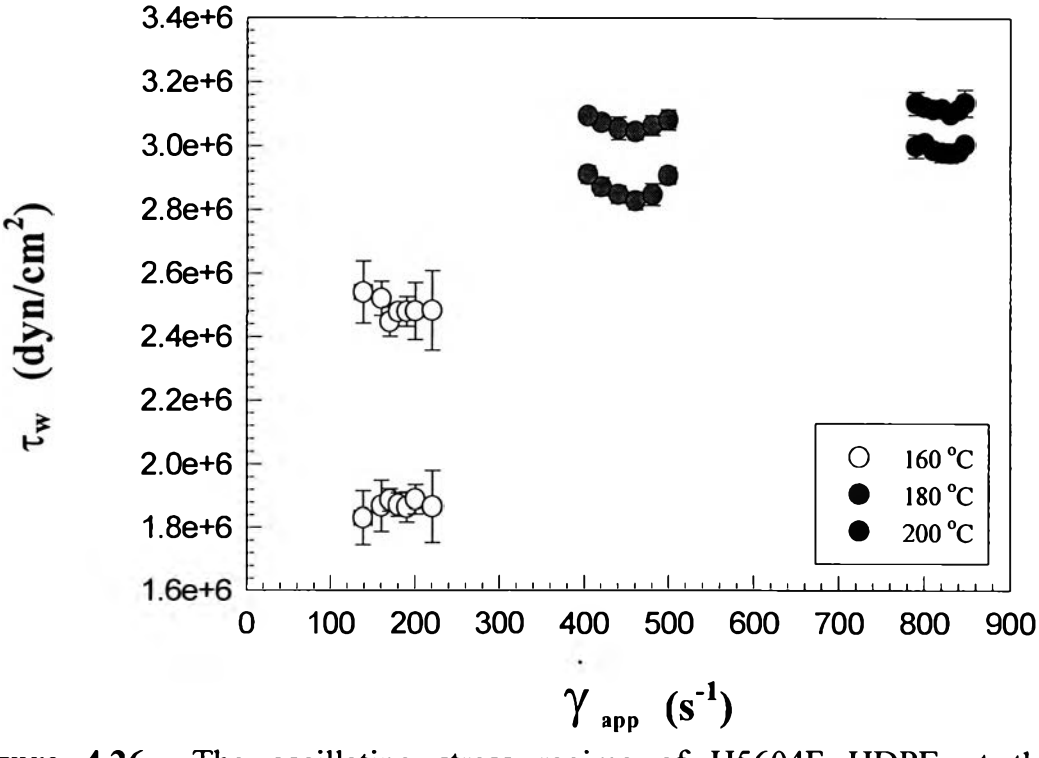

Figure 4.26 The oscillating stress regime of H5604F HDPE at the temperatures of 160, 180 and 200 ^{0}C.

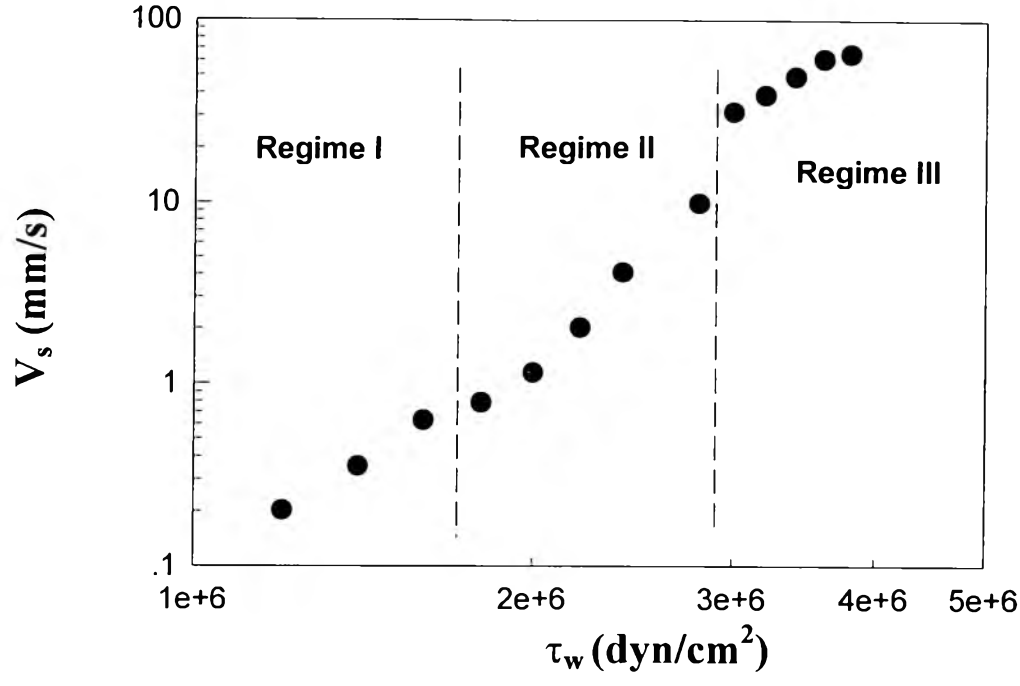

Figure 4.27a Slip velocity of H5604F HDPE as a function of shear stress at the temperature of 180 ^{0}C.

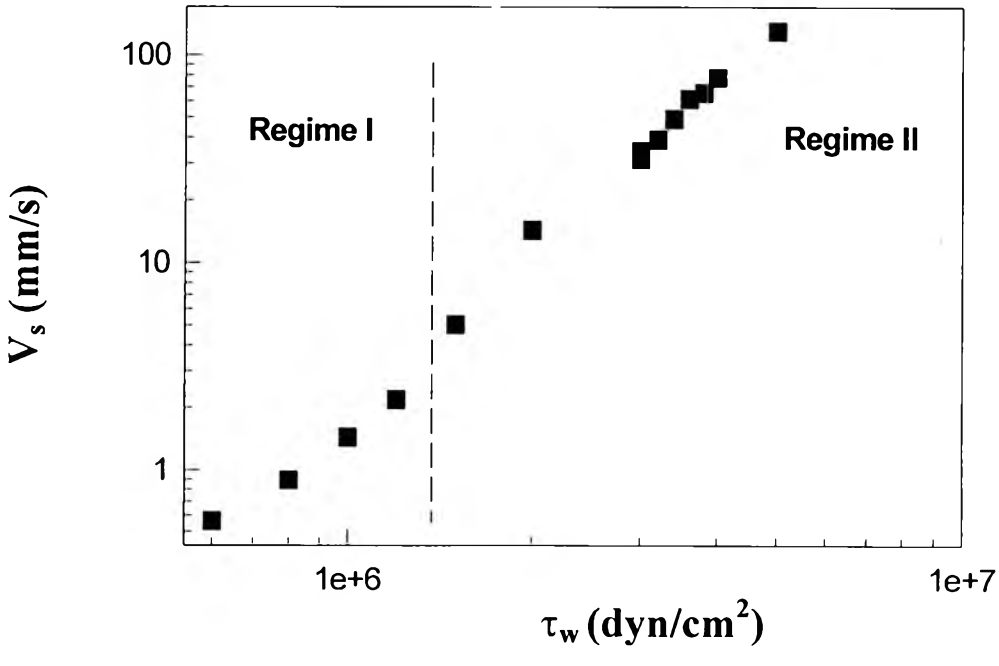

Figure 4.27b Slip velocity of H5840B HDPE as a function of shear stress at the temperature of 180 ^{0}C.

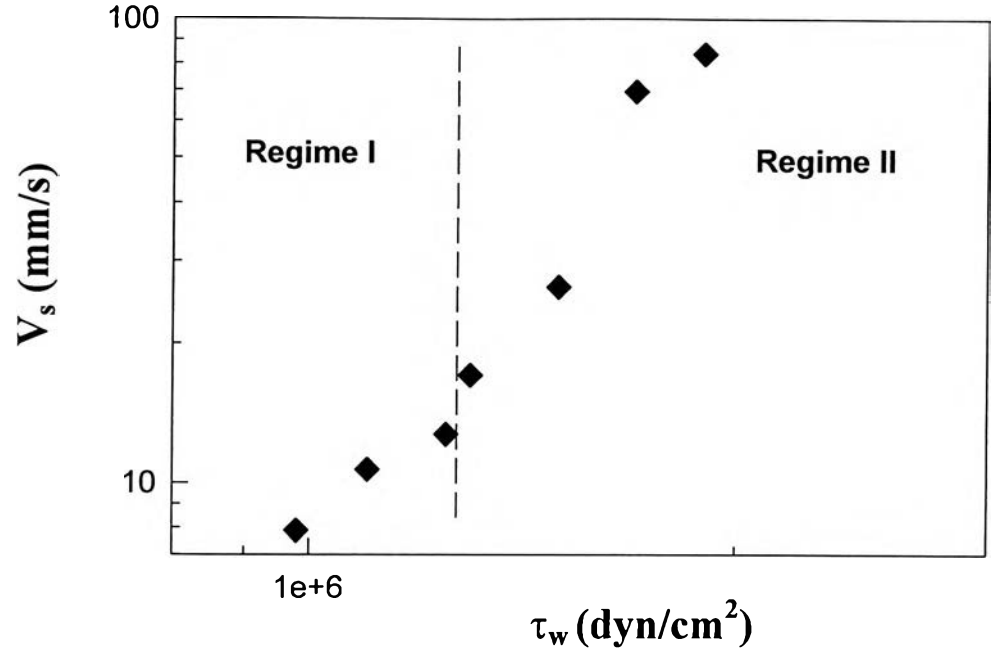

Figure 4.27c Slip velocity of H5818J HDPE as a function of shear stress at the temperature of 180 ^{0}C.

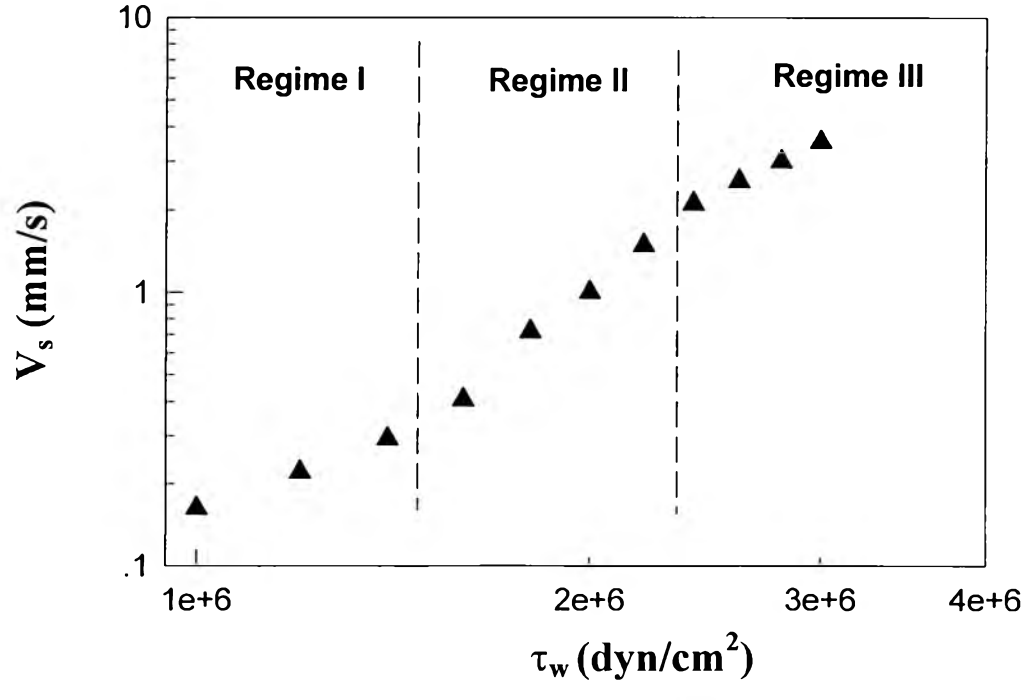

Figure 4.27d Slip velocity of H5690S HDPE as a function of shear stress at the temperature of 180 ^{0}C.

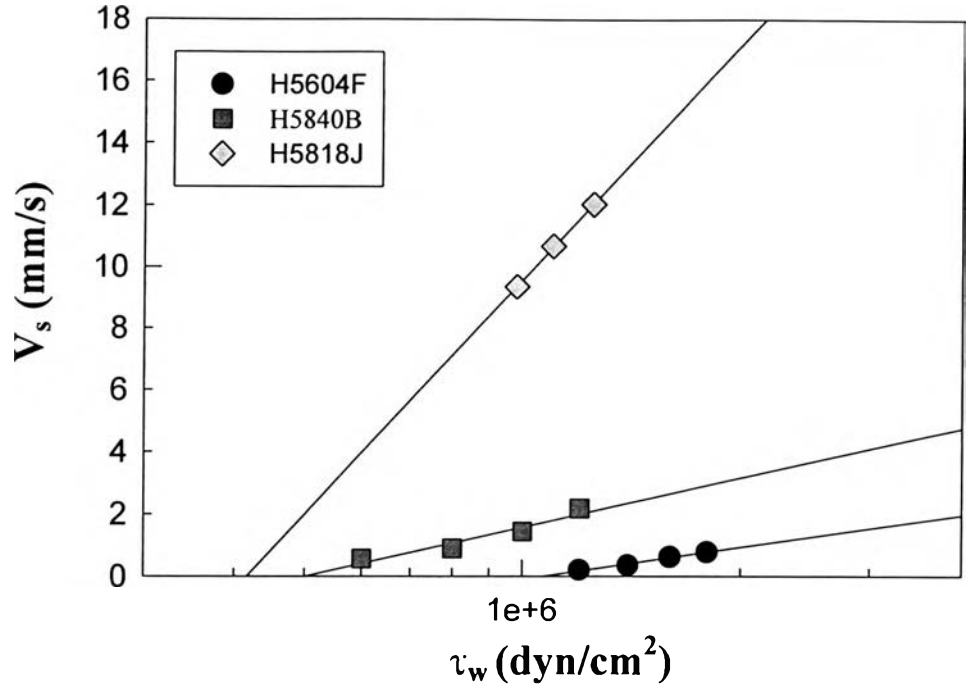

Figure 4.28 Critical shear stress of H5604F HDPE, H5840B HDPE and H5818J HDPE at the temperature of 180 ^{0}C.

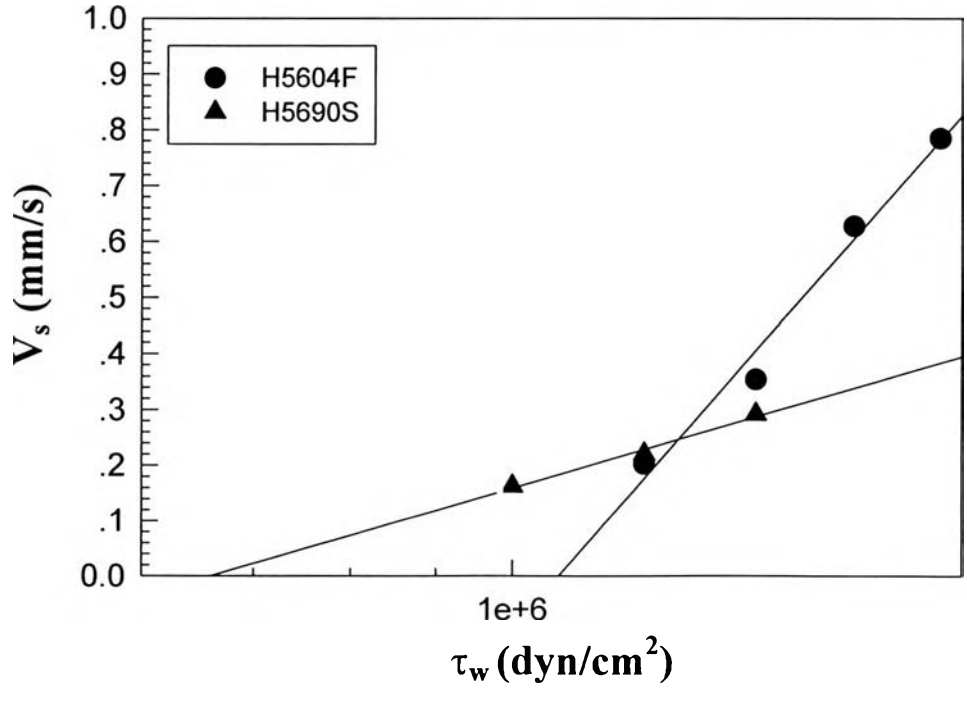

Figure 4.29 Critical shear stress of H5604F HDPE and H5690S HDPE at the temperature of 180 ^{0}C.

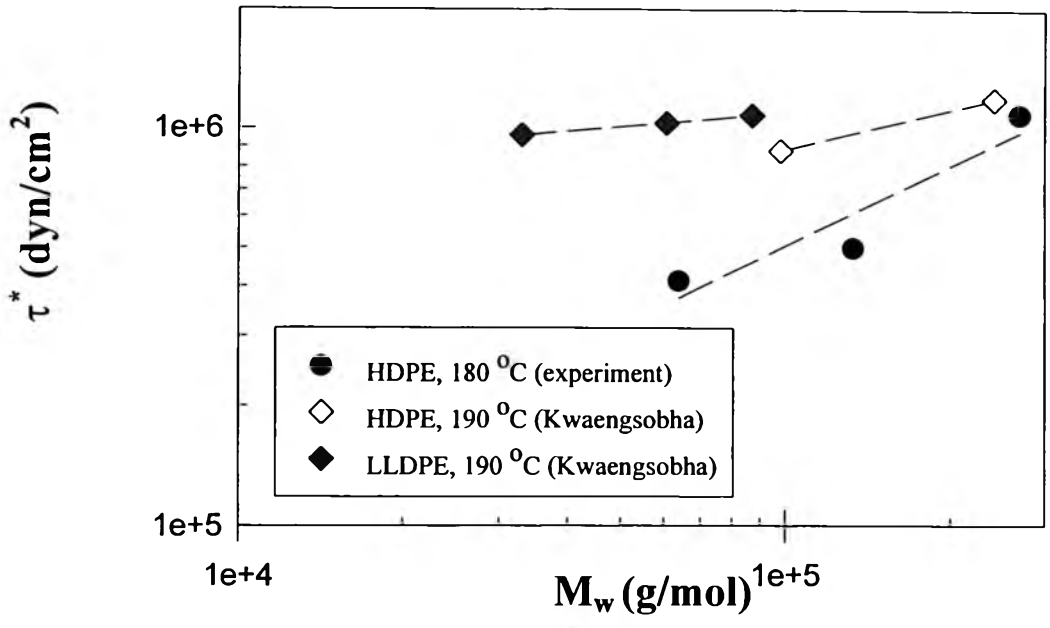

Figure 4.30 Critical shear stress as a function of molecular weight of three experiments: HDPE at 180 ^{0}C; HDPE at 190 ^{0}C (Kwaengsobha, 1998) and LLDPE at 190 ^{0}C (Kwaengsobha, 1998).

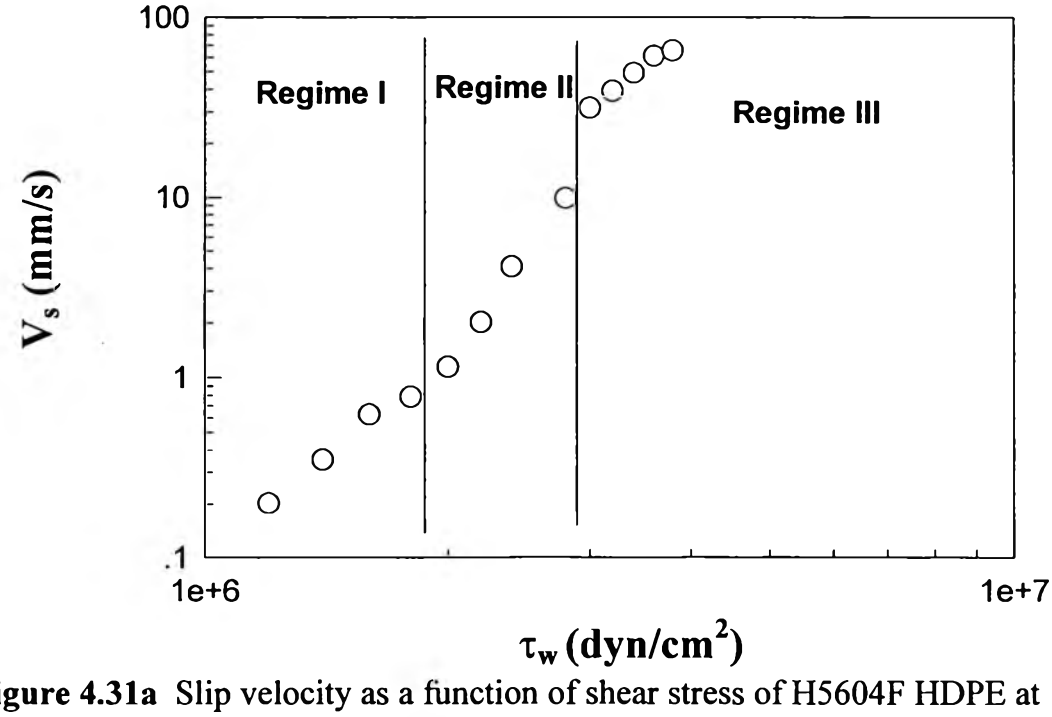

Figure 4.31a Slip velocity as a function of shear stress of H5604F HDPE at the temperature of 160 ^{0}C.

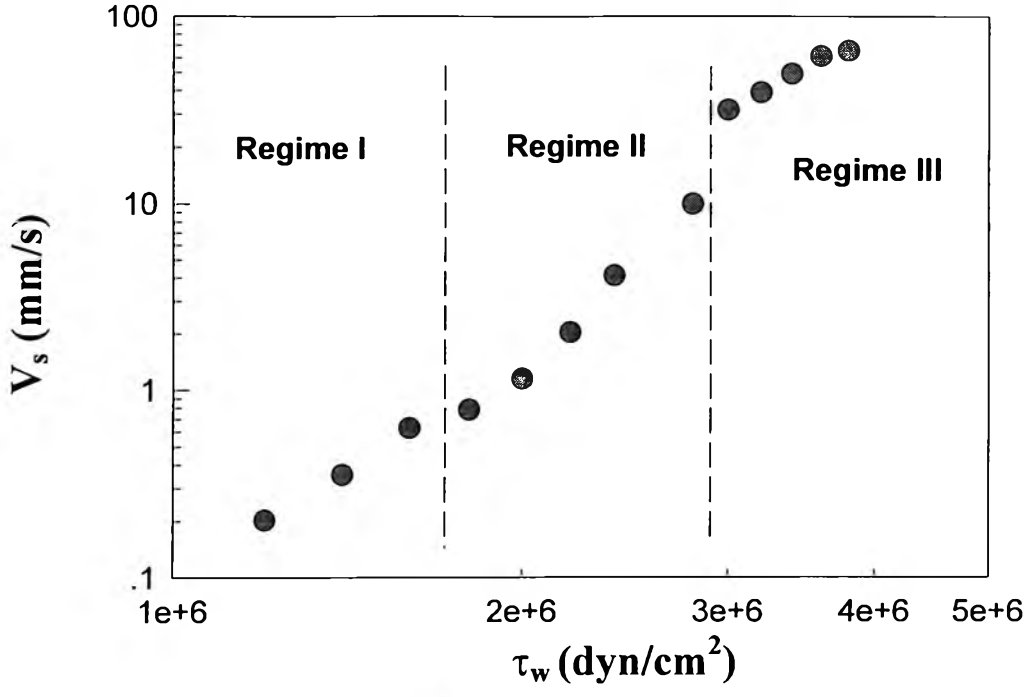

Figure 4.31b Slip velocity as a function of shear stress of H5604F HDPE at the temperature of 180 ^{0}C.

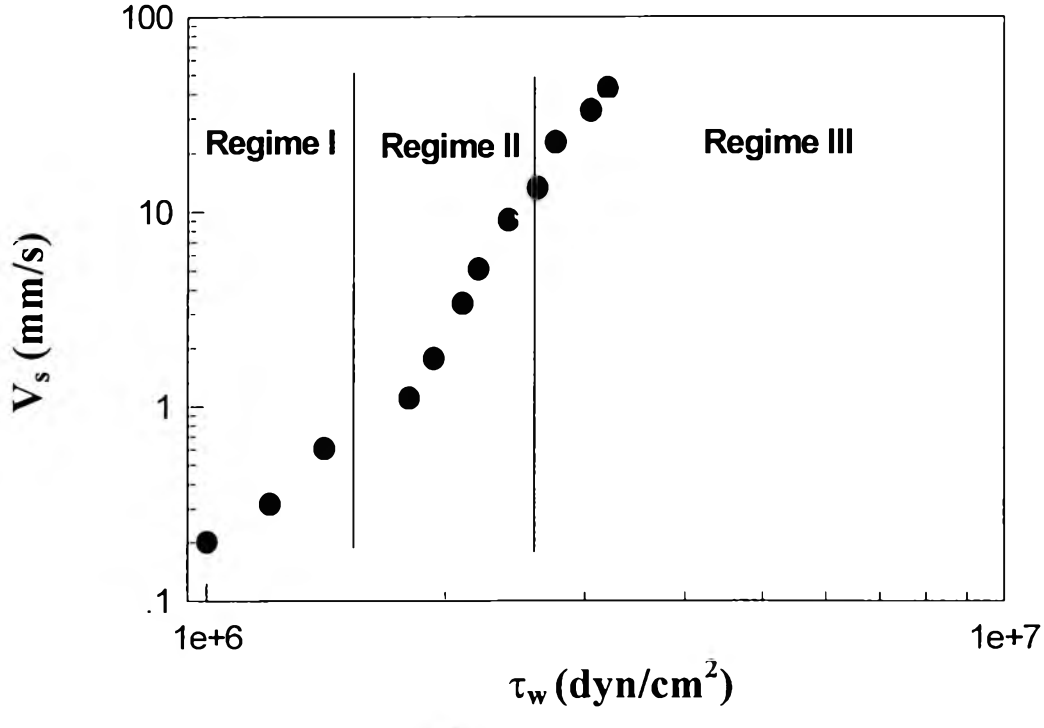

Figure 4.31c Slip velocity as a function of shear stress of H5604F HDPE at the temperature of 200 ^{0}C.

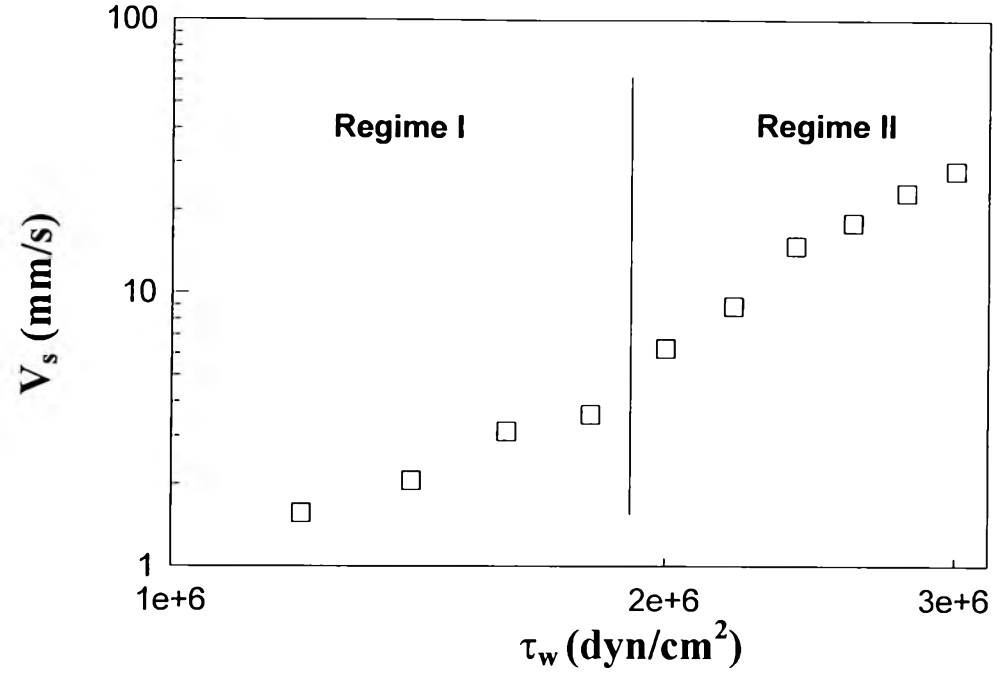

Figure 4.32a Slip velocity as a function of shear stress of H5840B HDPE at the temperature of 160 ^{0}C.

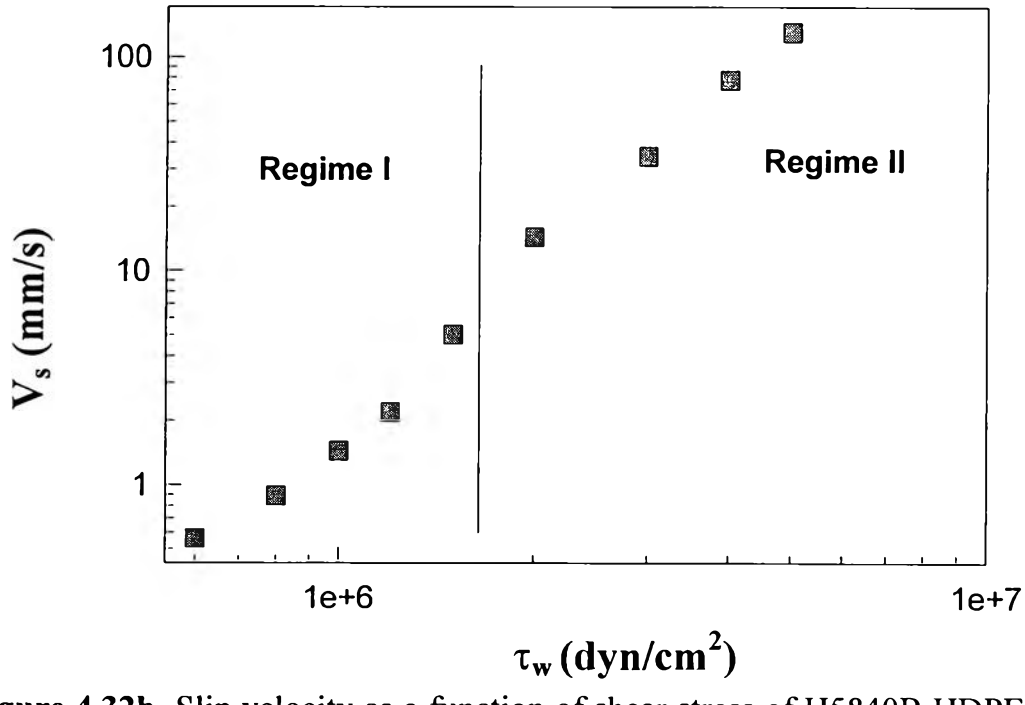

Figure 4.32b Slip velocity as a function of shear stress of H5840B HDPE at the temperature of 180 ^{0}C.

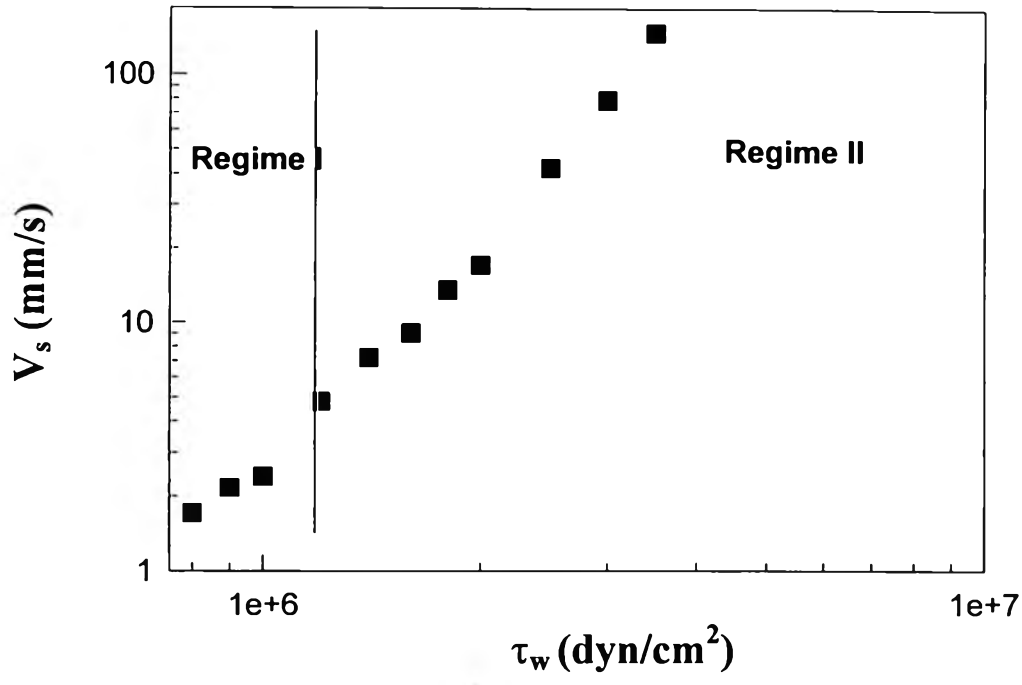

Figure 4.32c Slip velocity as a function of shear stress of H5840B HDPE at the temperature of 200 ^{0}C.

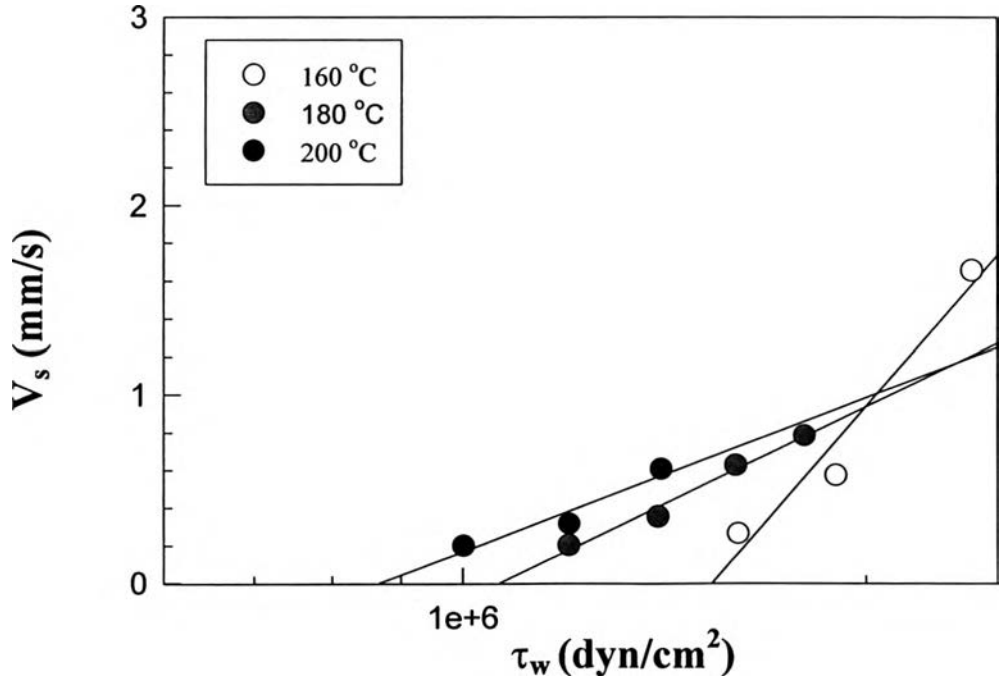

Figure 4.33 Critical shear stress of H5604F HDPE at the temperatures of 160, 180 and 200 ^{0}C.

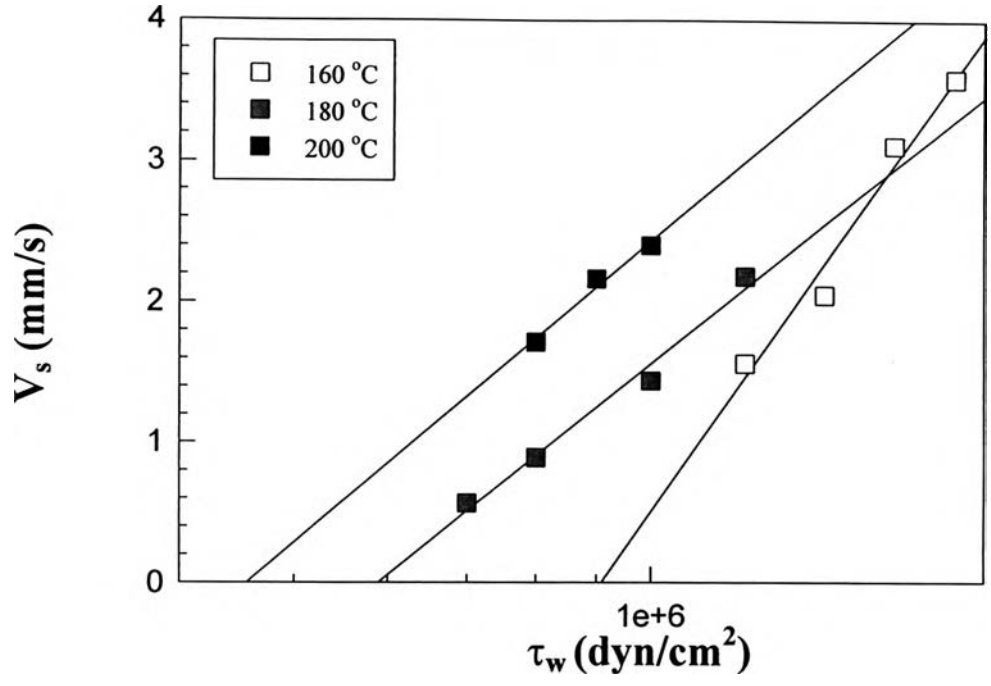

Figure 4.34 Critical shear stress of H5840B HDPE at the temperatures of 160, 180 and 200 ^{0}C.

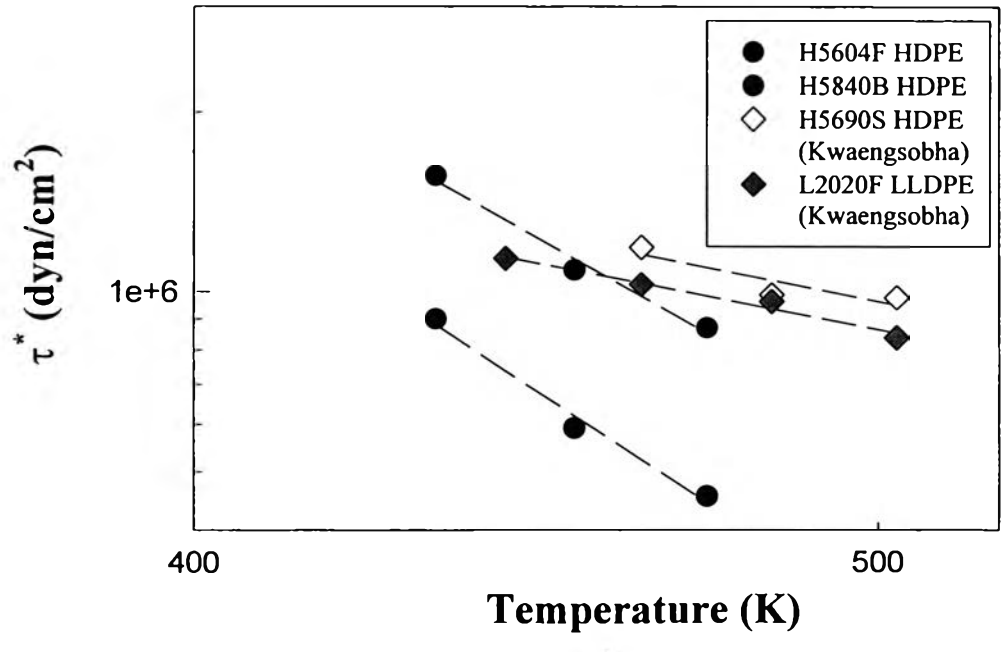

Figure 4.35 Critical shear stress as a function of temperature of four experiments: H5604F HDPE; H5840B HDPE; H5690S HDPE (Kwaengsobha, 1998) and L2020F LLDPE (Kwaengsobha, 1998) melts.

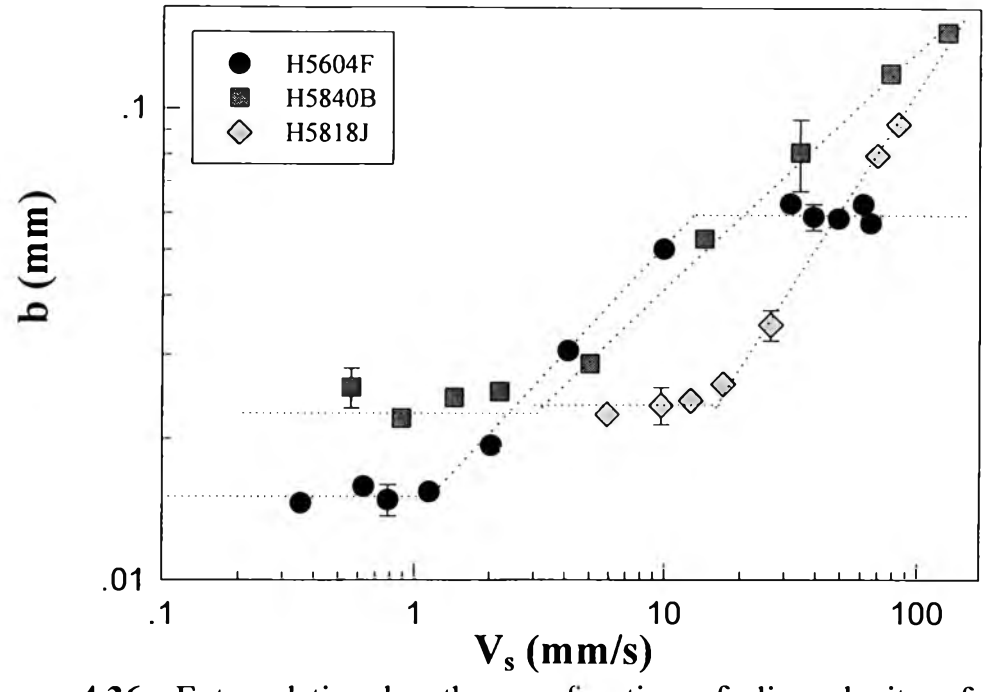

Figure 4.36 Extrapolation length as a function of slip velocity of three different molecular weights at the temperature of 180 ^{0}C.

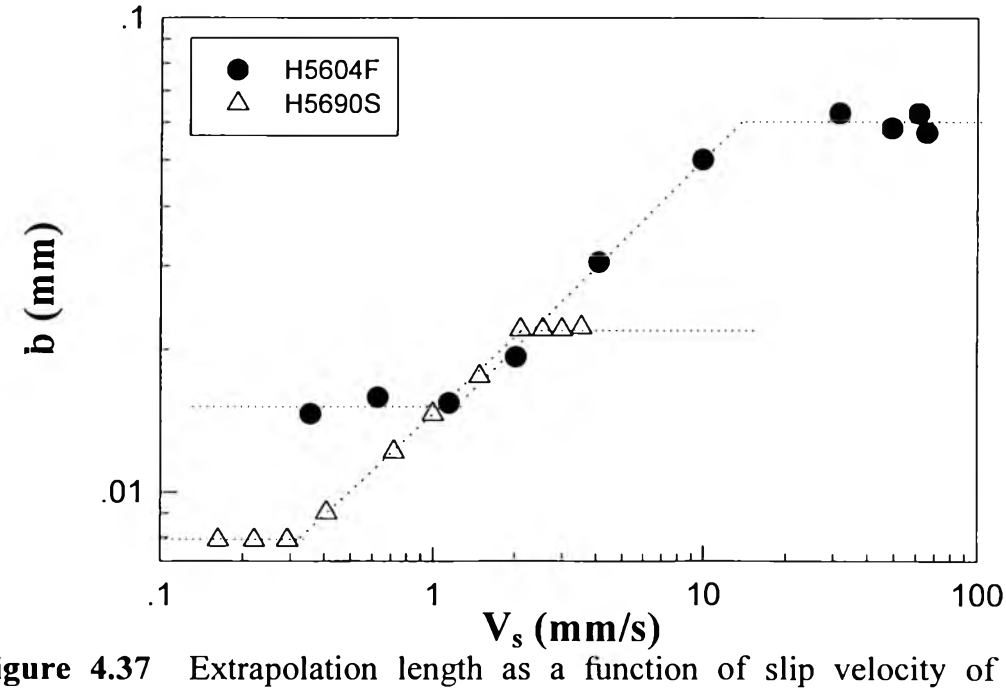

Figure 4.37 Extrapolation length as a function of slip velocity of two different polydispersities at the temperature of 180 ^{0}C.

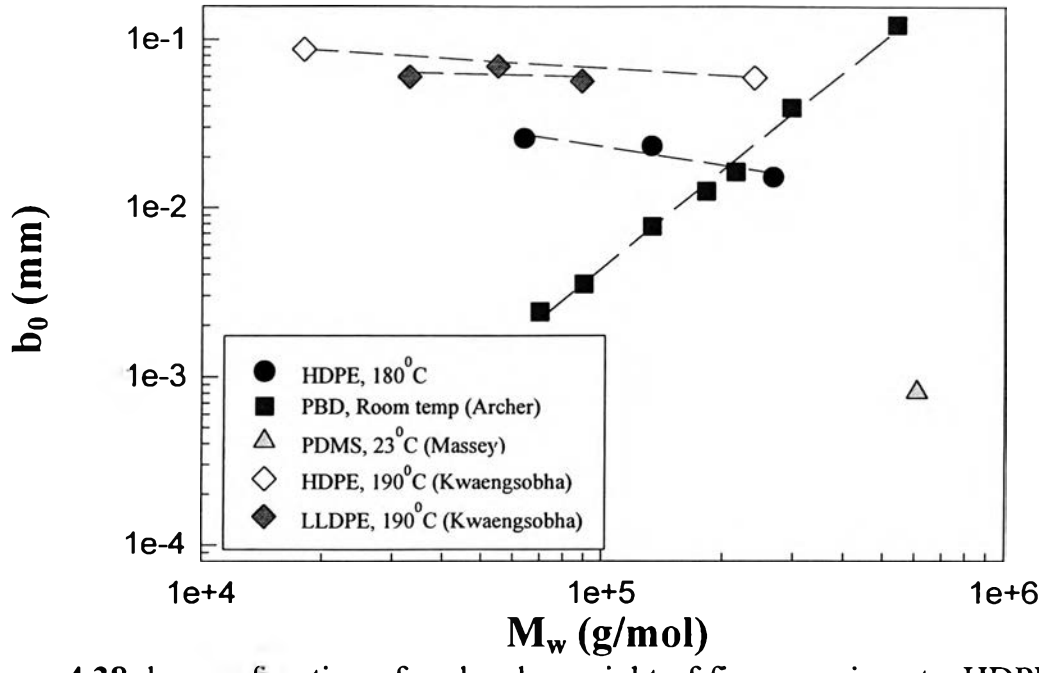

Figure 4.38 b_0 as a function of molecular weight of five experiments: HDPE at 180°C; PBD at room temperature (Archer, 1998); PDMS at 23°C (Massey, 1997); HDPE at 190 °C (Kwaengsobha, 1998) and LLDPE at 190 °C (Kwaengsobha, 1998).

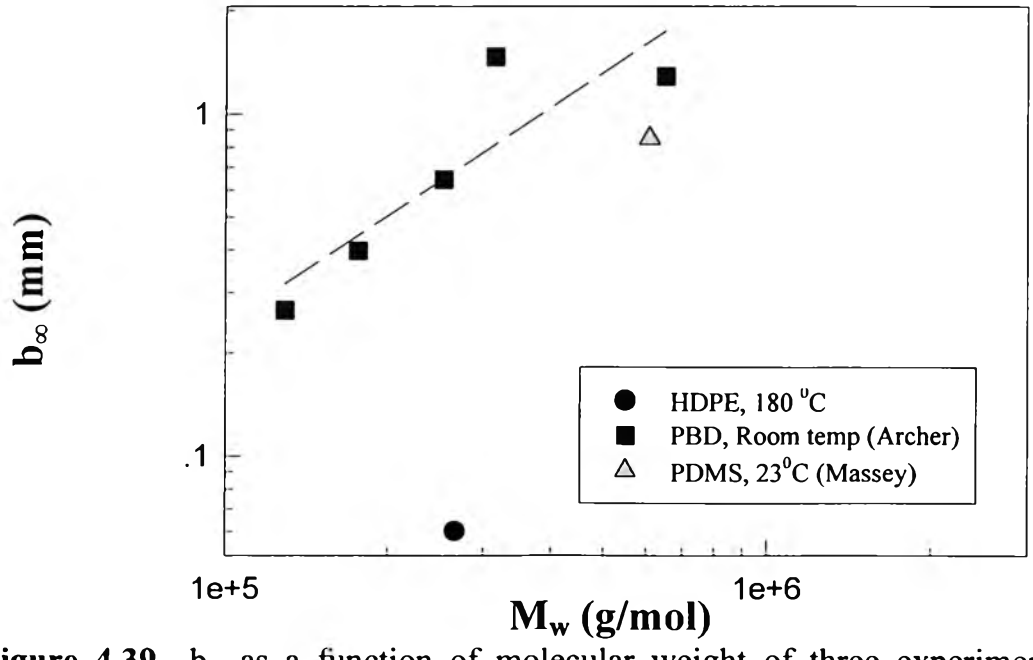

Figure 4.39 b_∞ as a function of molecular weight of three experiments: HDPE at 180°C; PBD at room temperature (Archer, 1998) and PDMS at 23°C (Massey, 1997).

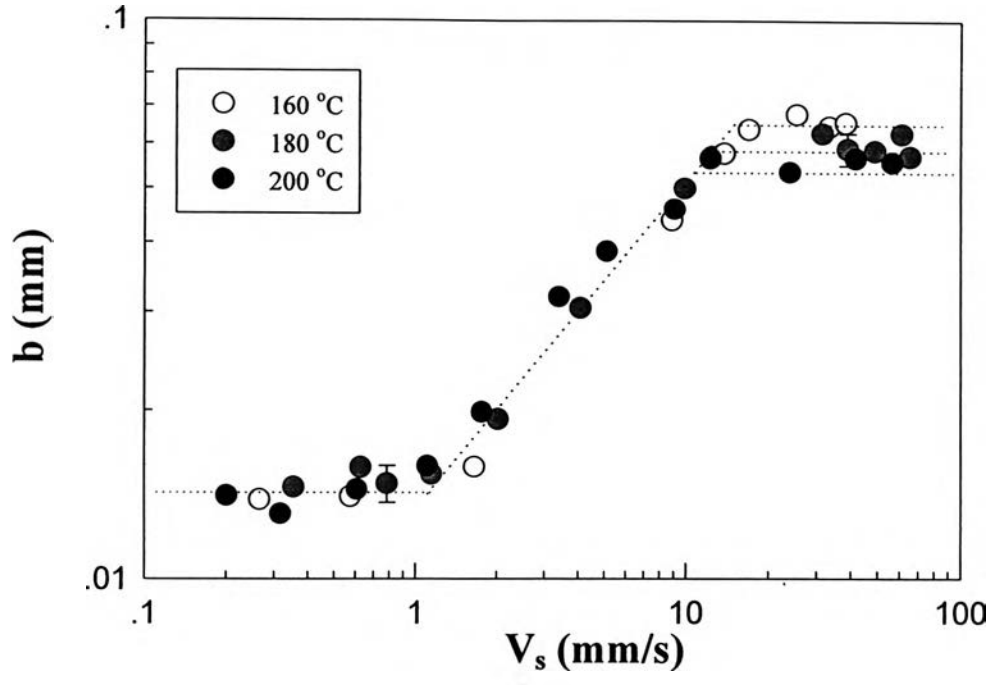

Figure 4.40 Extrapolation length as a function of slip velocity of H5604F HDPE at the temperatures of 160, 180 and 200 ^{0}C.

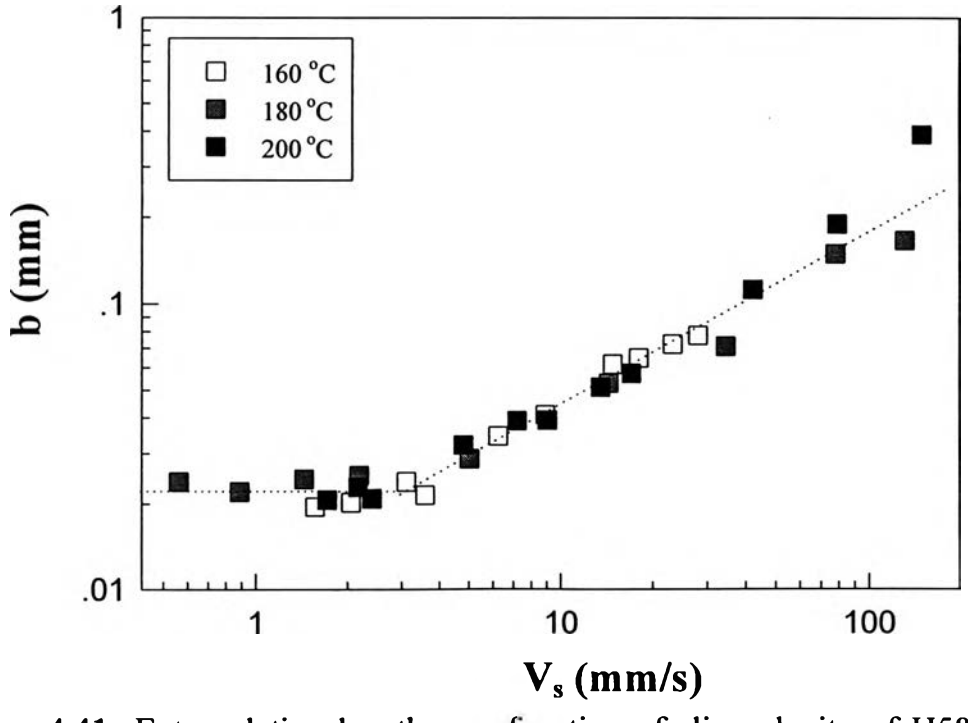

Figure 4.41 Extrapolation length as a function of slip velocity of H5840B HDPE at the temperatures of 160, 180 and 200 ^{0}C.

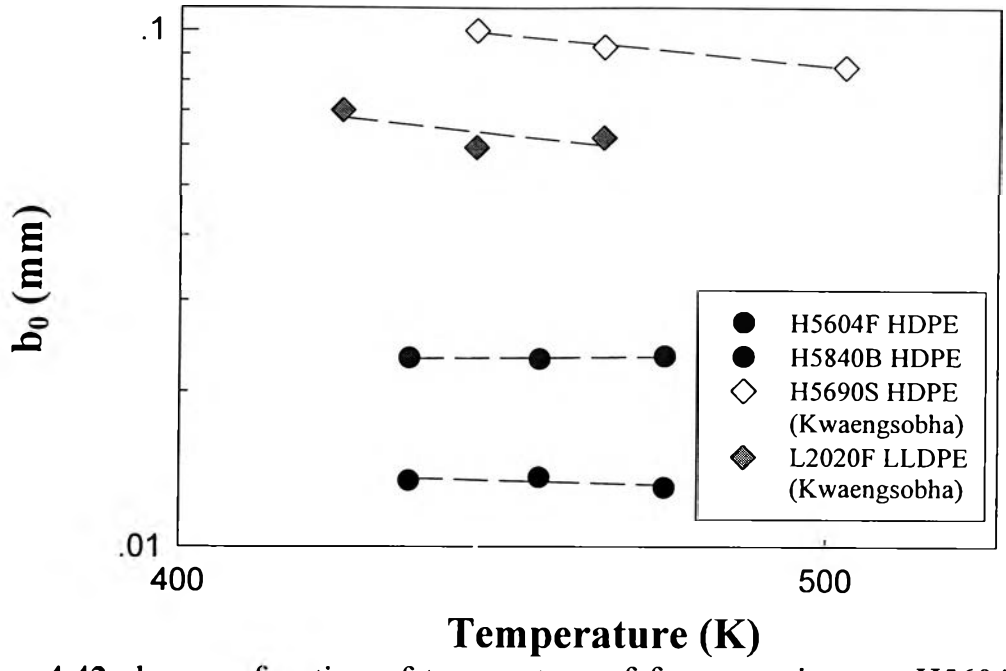

Figure 4.42 b_0 as a function of temperature of four experiments: H5604F HDPE; H5840B HDPE; H5690S HDPE (Kwaengsobha, 1998) and L2020F LLDPE (Kwaengsobha, 1998).

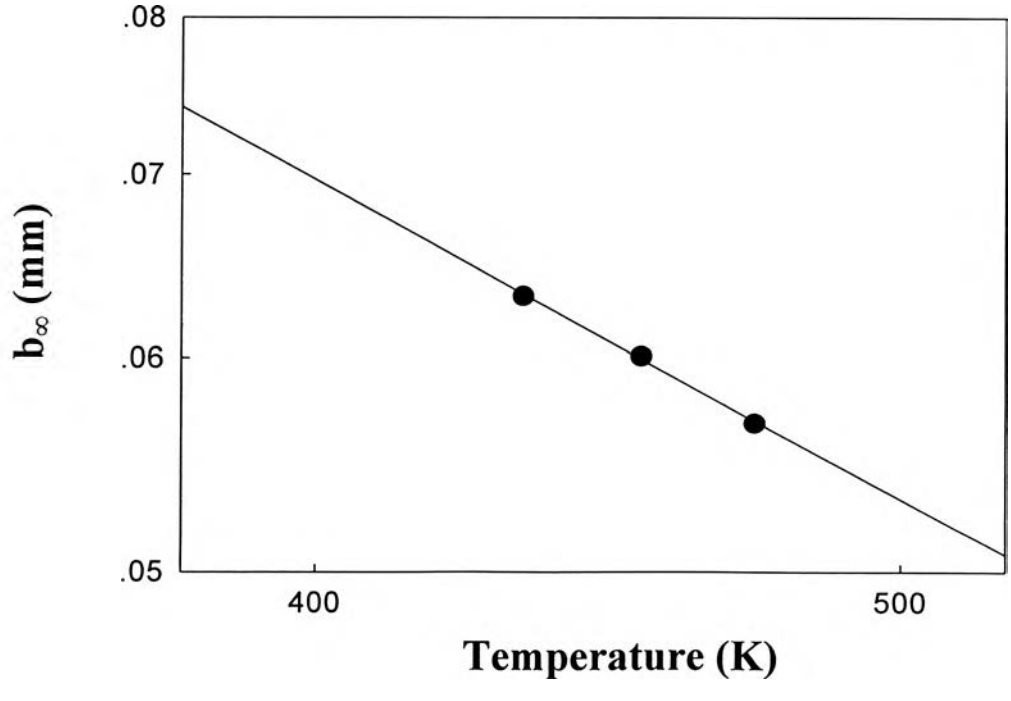

Figure 4.43 b_∞ as a function of temperature of H5604F HDPE at the temperatures of 160, 180 and 200 ^{0}C.

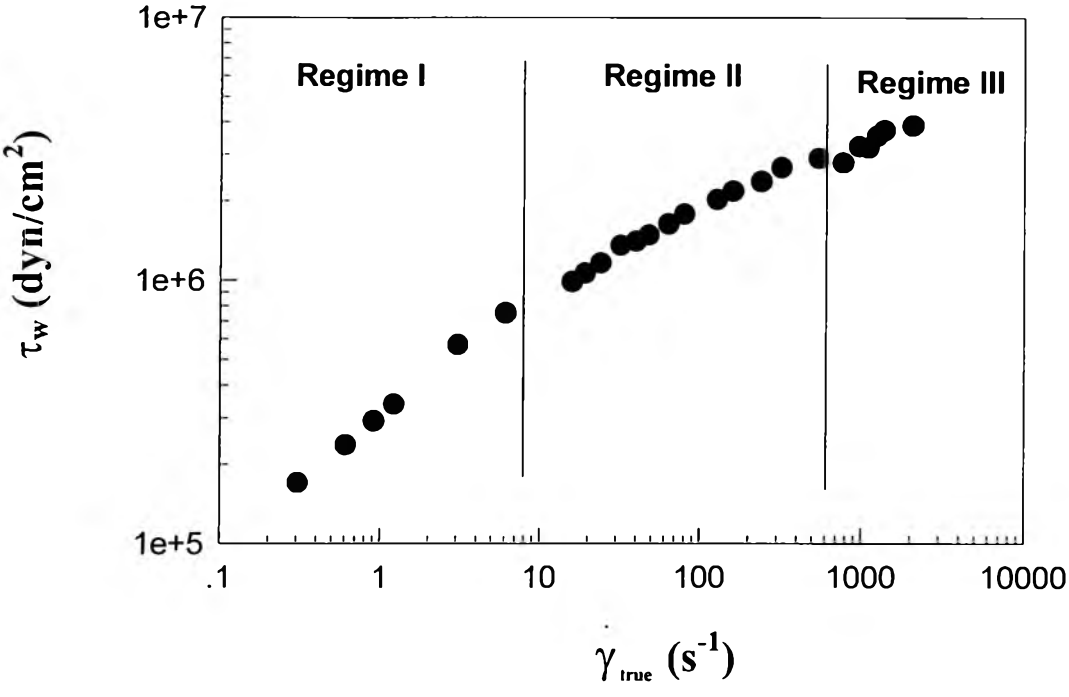

Figure 4.44 The true flow curve of H5604F HDPE at the temperature of 180 ^{0}C.

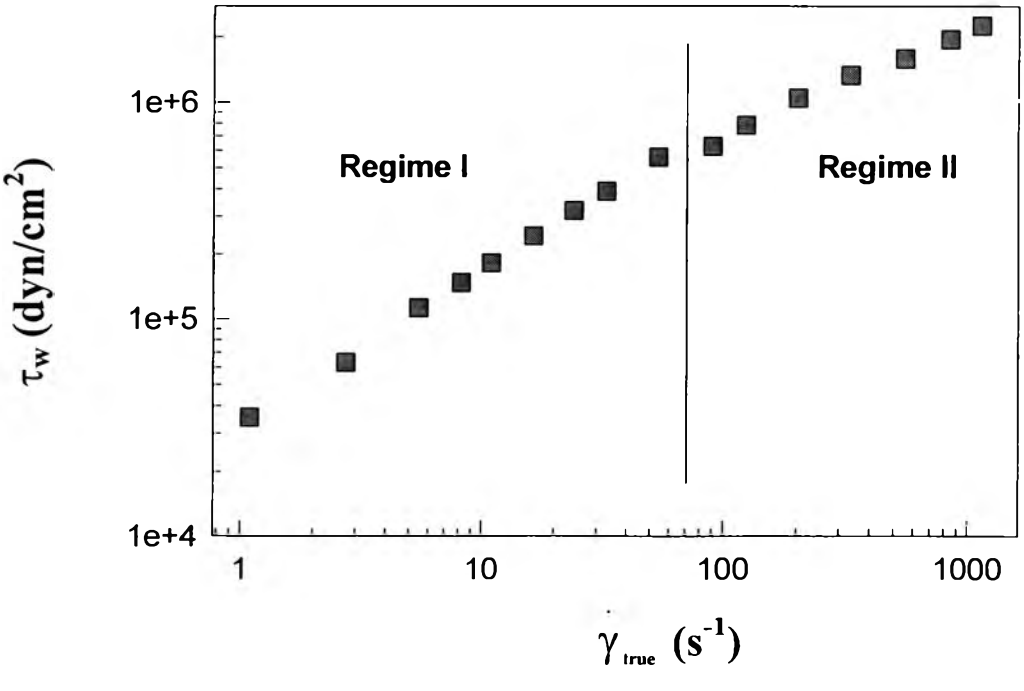

Figure 4.45 The true flow curve of H5840B HDPE at the temperature of 180 ^{0}C.

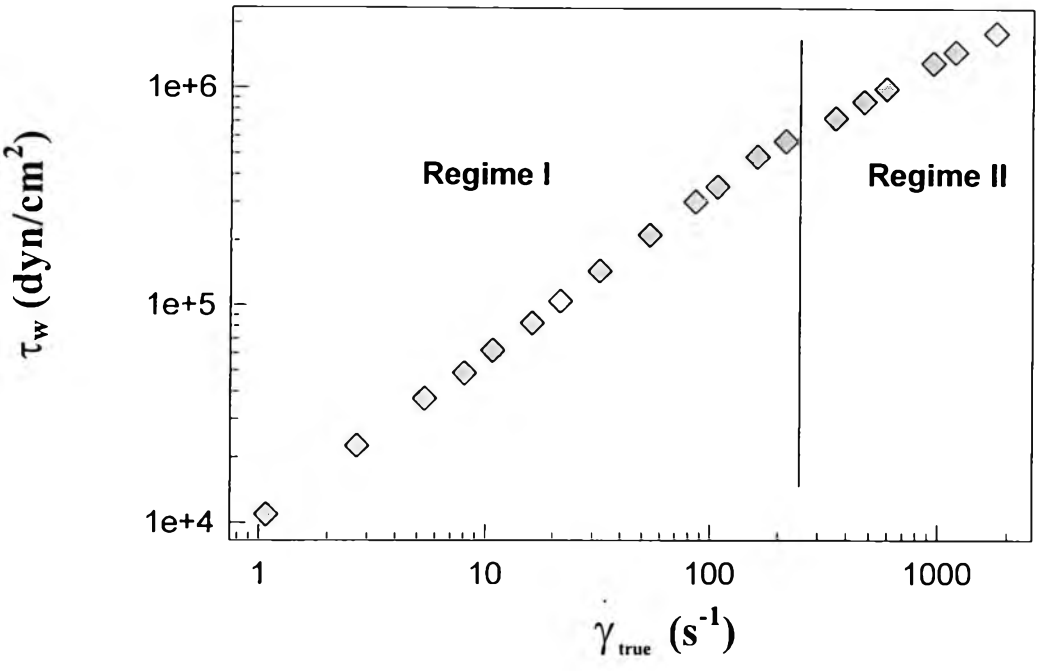

Figure 4.46 The true flow curve of H5818J HDPE at the temperature of 180 ^{0}C.

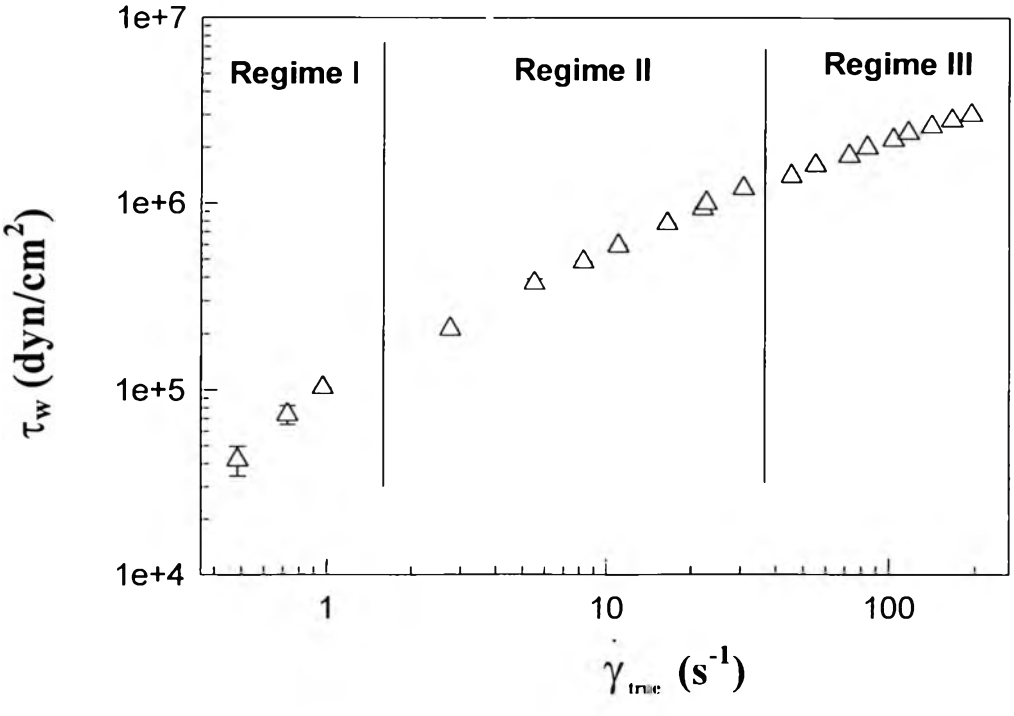

Figure 4.47 The true flow curve of H5690S HDPE at the temperature of 180 ^{0}C.

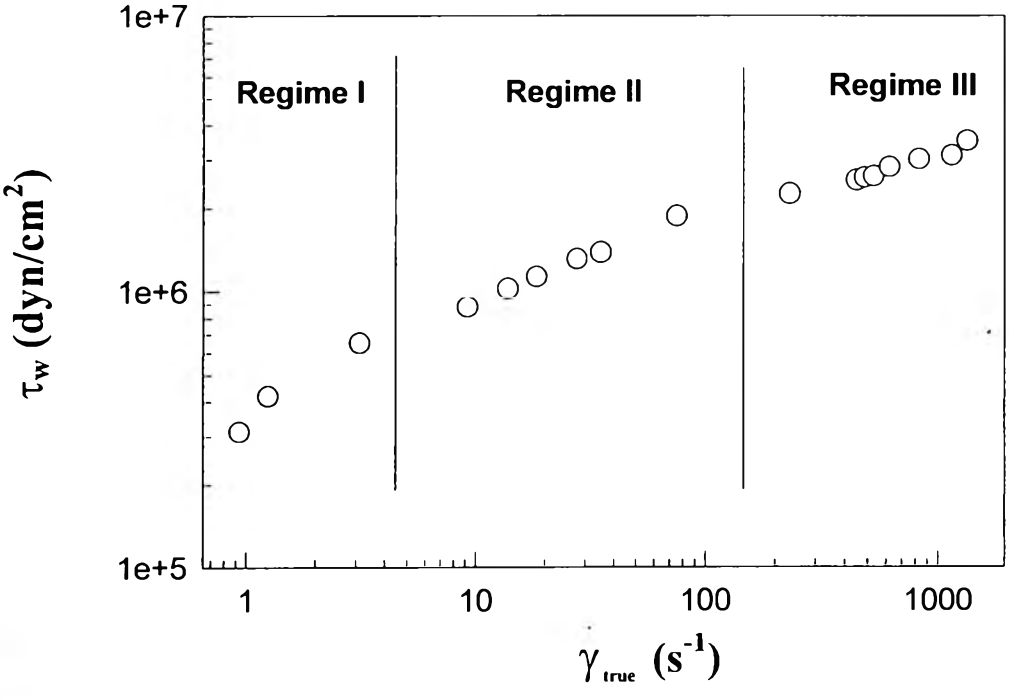

Figure 4.48 The true flow curve of H5604F HDPE at the temperature of 160 ^{0}C.

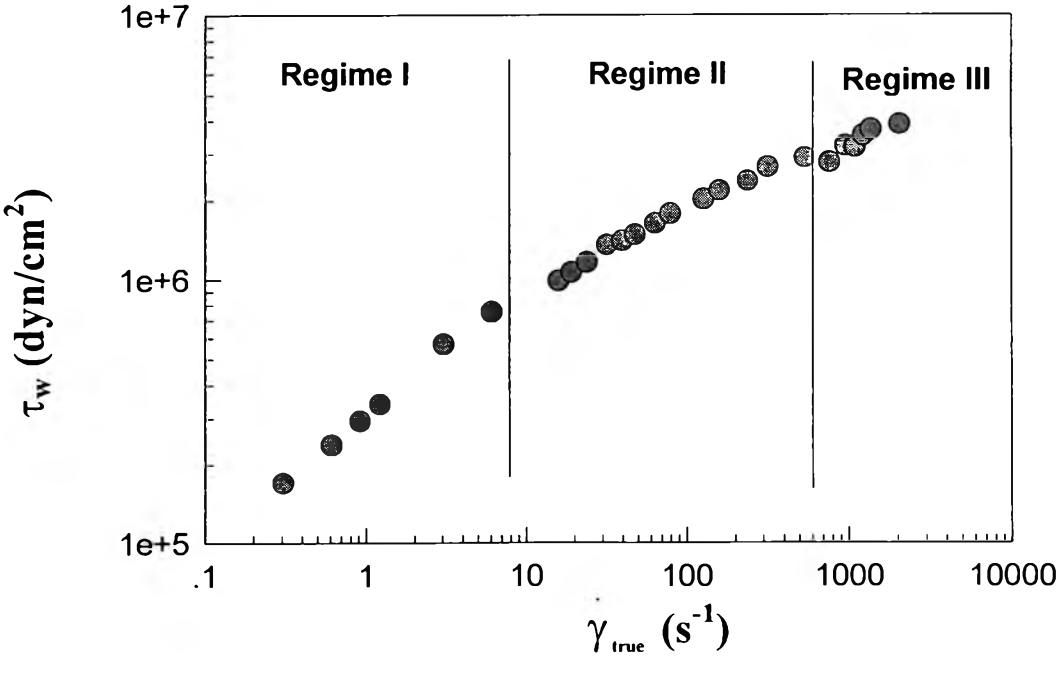

Figure 4.49 The true flow curve of H5604F HDPE at the temperature of 180 ^{0}C.

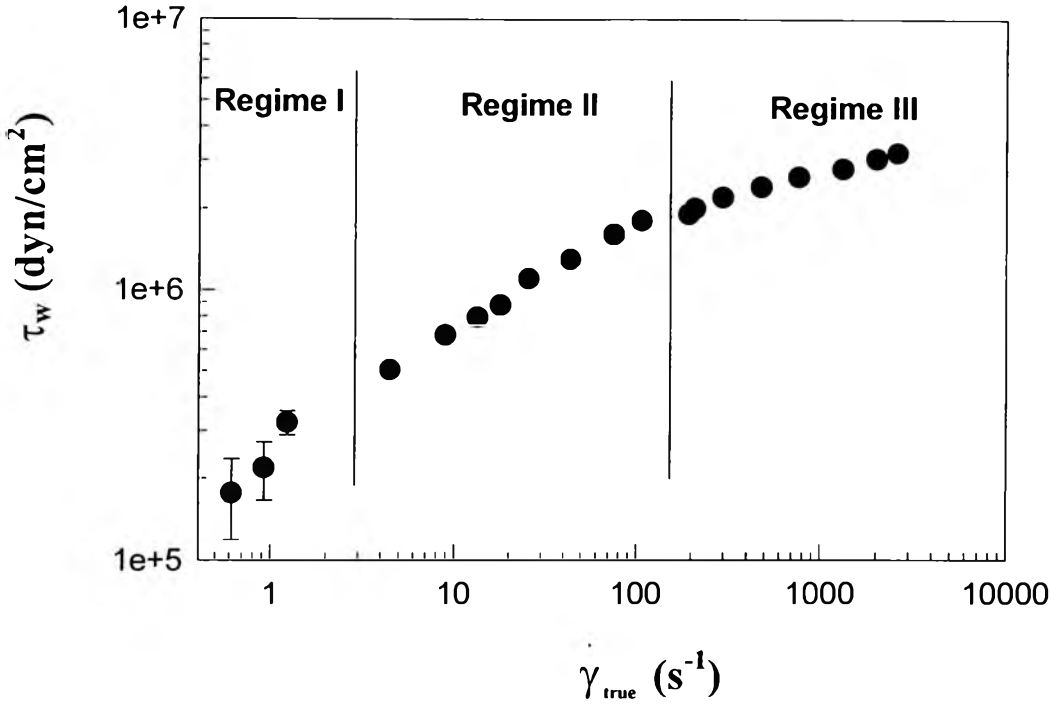

Figure 4.50 The true flow curve of H5604F HDPE at the temperature of 200 ^{0}C.

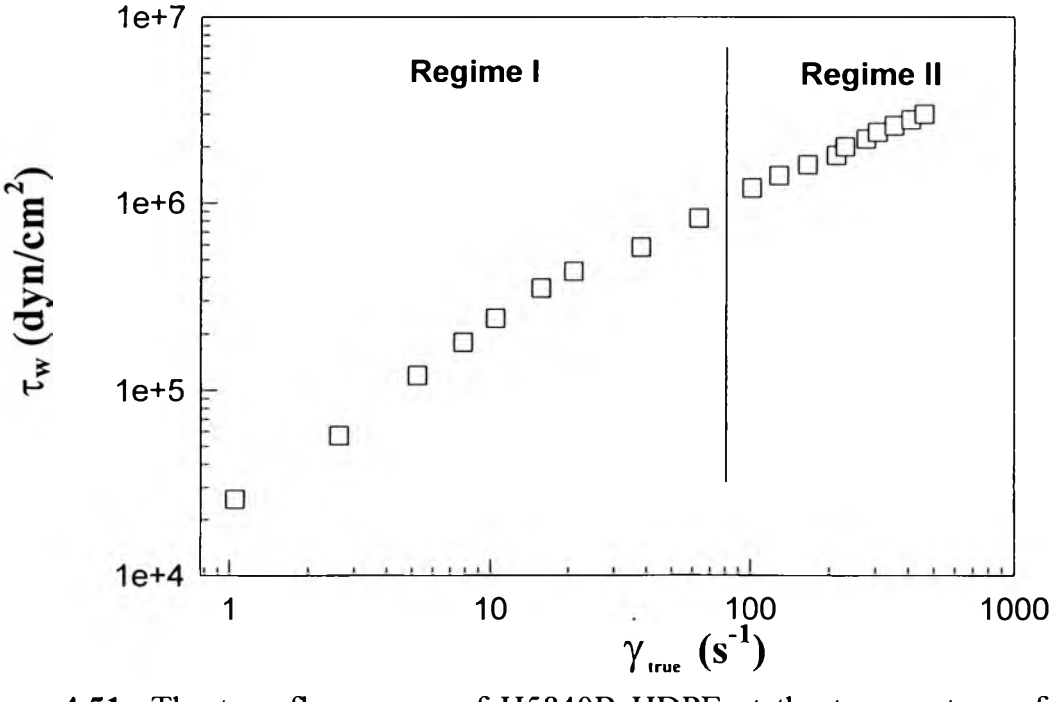

Figure 4.51 The true flow curve of H5840B HDPE at the temperature of 160 ^{0}C.

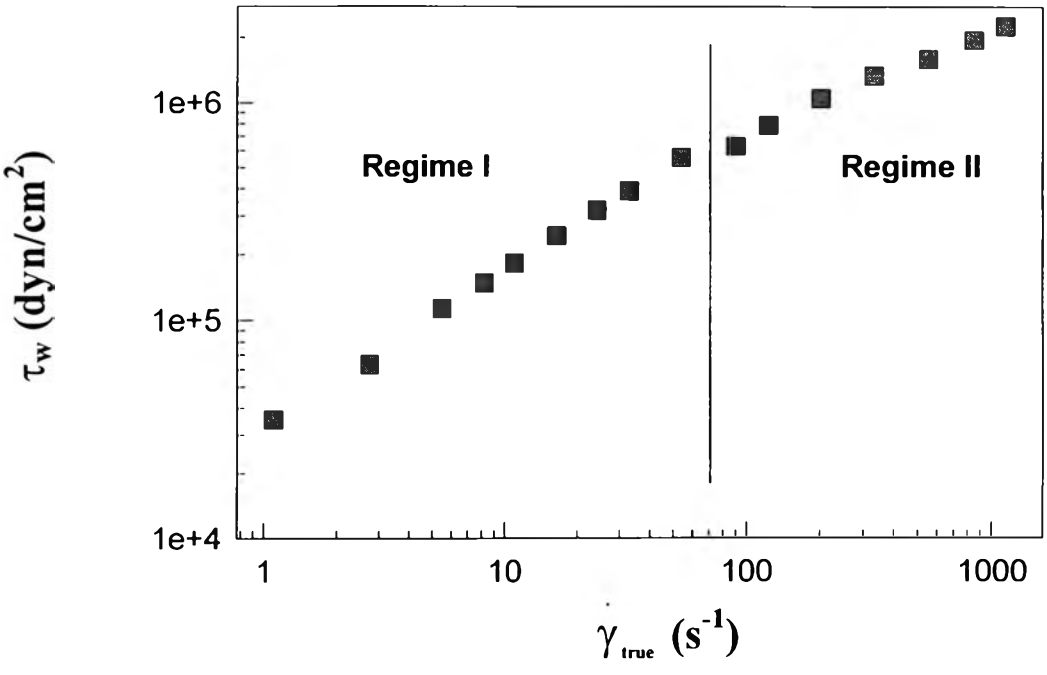

Figure 4.52 The true flow curve of H5840B HDPE at the temperature of 180 ^{0}C.

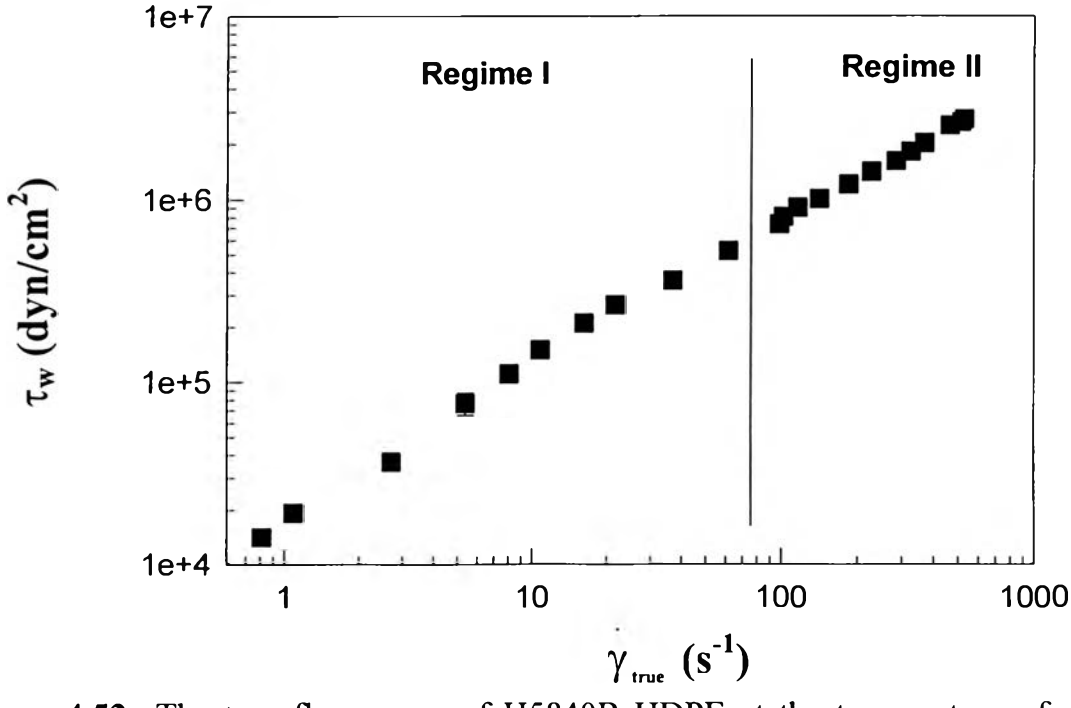

Figure 4.53 The true flow curve of H5840B HDPE at the temperature of 200 ^{0}C.

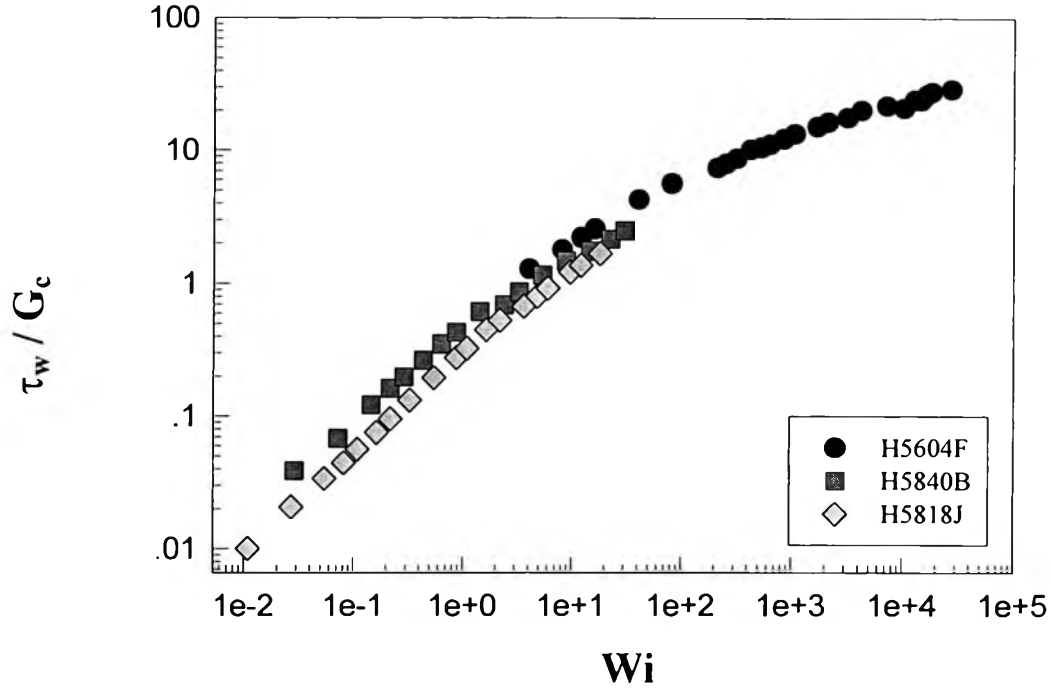

Figure 4.54 The normalized flow curves of three HDPE (H5604F, H5840B and H5818J) melts of different molecular weight at the temperature of 180 ^{0}C.

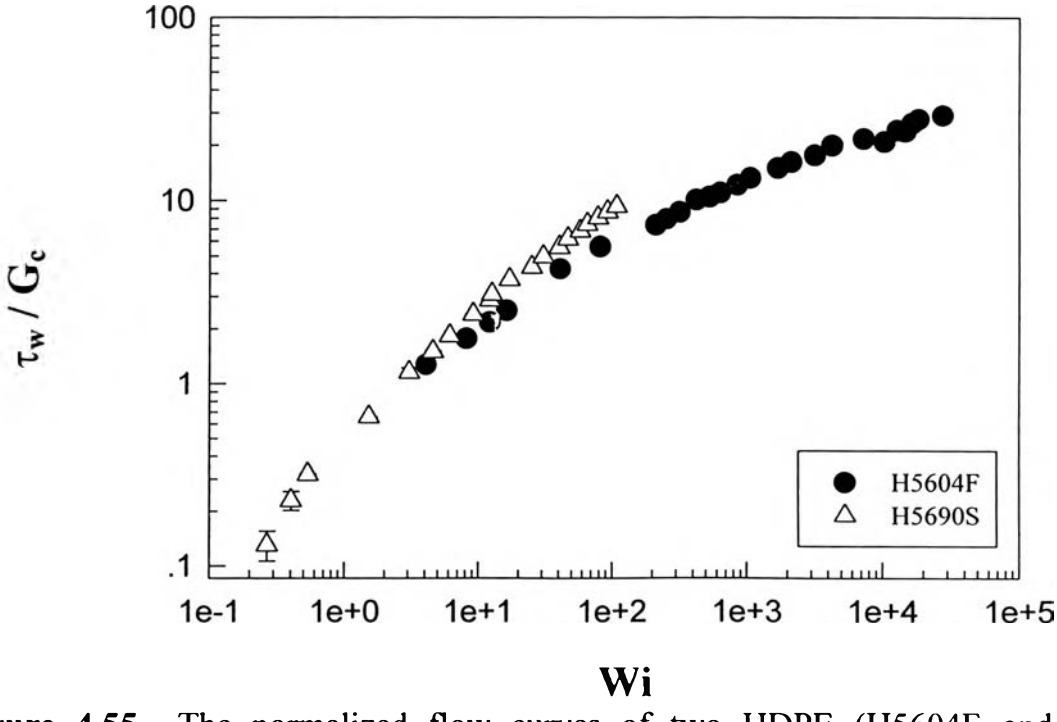

Figure 4.55 The normalized flow curves of two HDPE (H5604F and H5690S) melts of different polydispersity at the temperature of 180 ^{0}C.

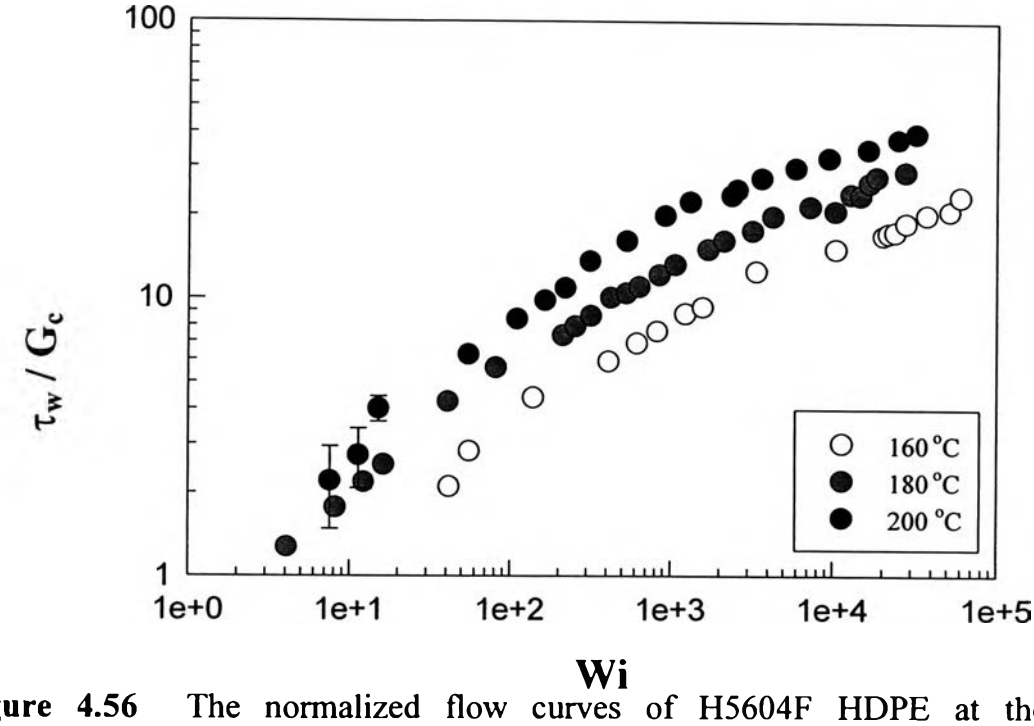

Figure 4.56 The normalized flow curves of H5604F HDPE at the temperatures of 160, 180 and 200 ^{0}C.

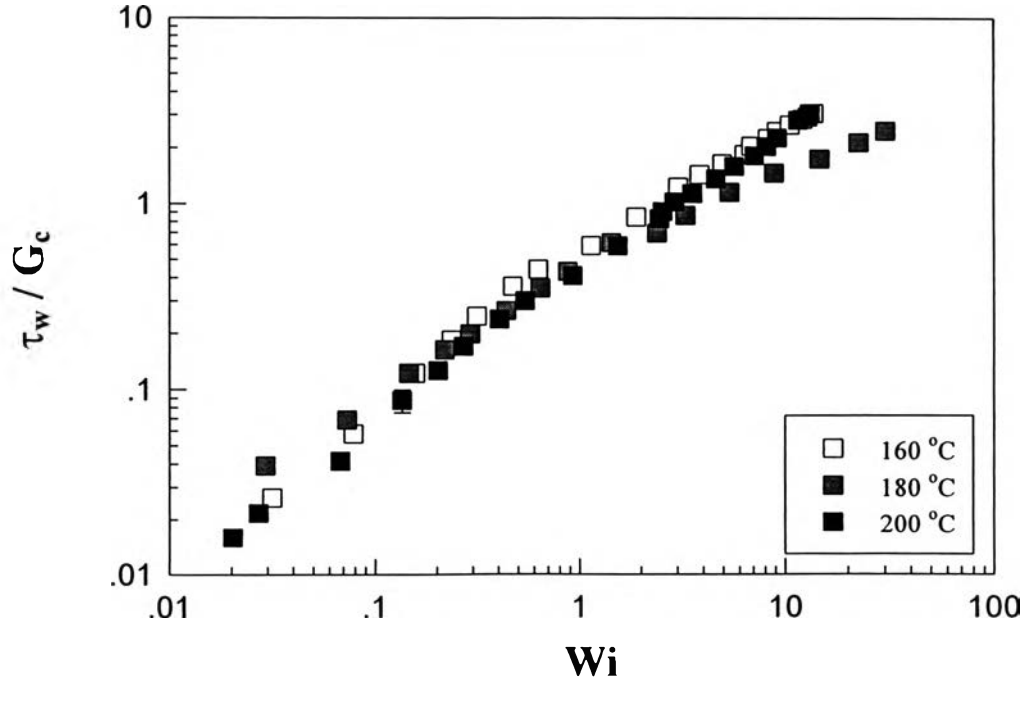

Figure 4.57 The normalized flow curves of H5840B HDPE at the temperatures of 160, 180 and 200 ^{0}C.